Fetal estrogens are not involved in sex determination but critical for early ovarian differentiation in rabbits.

Geneviève Jolivet[1*], Nathalie Daniel-Carlier[1], Erwana Harscoët[1], Eloïse Airaud[1], Aurélie Dewaele[1], Cloé Pierson[1], Frank Giton[2], Laurent Boulanger[1], Nathalie Daniel[1], Béatrice Mandon-Pépin[1], Maëlle Pannetier[1], Eric Pailhoux[1]

[1] Université Paris-Saclay, INRAE, ENVA, UVSQ, BREED, 78350, Jouy-en-Josas, France

[2] AP-HP, Pôle biologie-Pathologie Henri Mondor, Créteil, France; INSERM IMRB U955, Créteil, France

*Corresponding author

Key words: CYP26A1, AROMATASE, sex determination, ovary, rabbit, TALEN

Abstract

AROMATASE, encoded by the *CYP19A1* gene, is the cytochrome enzyme responsible for the synthesis of estrogens in vertebrates. In most mammals a peak of expression of the *CYP19A1* gene occurs in the fetal XX gonad when sexual differentiation starts up. To elucidate the role of this peak, we produced 3 lines of TALEN genetically edited *CYP19A1* KO rabbits, that were void of any production of estradiol. All KO XX rabbits developed as females, with aberrantly small sized ovaries at adulthood, an almost empty reserve of primordial follicles and very few large antrum follicles. Ovulation never occurred. Our histological, immunohistological and transcriptomic analyses showed that the surge of estradiol in the XX fetal rabbit gonad is dispensable for its determination as an ovary, or for meiosis. However, it is mandatory for the high proliferation and differentiation of both somatic and germ cells, and consequently for the establishment of the ovarian reserve.

In Vertebrates, AROMATASE is the unique enzyme responsible for the synthesis of estrogens. It converts specifically three androgenic substrates (androstenedione, testosterone and 17alpha-testosterone) to estrone, estradiol, and estriol respectively. It is the product of the *CYP19A1* gene, which is the unique member of its gene family. Although the *CYP19A1* gene is commonly known to be mainly expressed by gonads in adults, a physiologically significant expression has already been reported in numerous tissues or organs such as bones, adipose tissue, brain or placenta (the expression in the latter depending on the species, see for review in (Conley and Hinshelwood 2001) and references herein).

In mammals, the expression of the *CYP19A1* gene begins early at around implantation in the embryo in rabbits (Dickmann *et al.* 1975; George and Wilson 1978b), pigs and ruminants (Gadsby *et al.* 1980). A second burst of expression was reported later in fetal life in the ovaries shortly after the sex determination process. This was described in rabbits (George *et al.* 1978; George and Wilson 1978b; Gondos *et al.* 1983; Daniel-Carlier *et al.* 2013), sheep (Mauleon *et al.* 1977; Payen *et al.* 1996; Torley *et al.* 2011), goats (Pannetier *et al.* 2006), bovines (Shemesh 1980; Ross *et al.* 2009; Garverick *et al.* 2010) and humans (George and Wilson 1978a) by RNA measurements or by estrogen assays in gonads or gonadal culture media. This peak is transitory and spans until meiosis initiation. Later on, *CYP19A1* gene expression increases progressively with follicle differentiation. It culminates in antrum follicles, the mural granulosa cells being the site of expression. By the past, the physiological significance of this fetal peak of expression has been searched in the rabbit species. Namely, George et al (George *et al.* 1978) have supposed that the local production of estrogens in the XX gonad was a key event for the initiation of the differentiation of the female fetal gonad but this hypothesis has still not been proven. In birds (Elbrecht and Smith 1992; Vaillant *et al.* 2001) and fishes (Guiguen *et al.* 2010), it was shown that estrogens are major determinants of the ovary orientation of the undifferentiated gonad in fetal or larval life. The question was thus to investigate the role of the fetal peak of estrogen in the mammalian gonad and more specifically to search whether in mammals it is mandatory for ovary differentiation.

To reach this aim, we decided to suppress the expression of the *CYP19A1* gene in a mammal species other than the mice. Indeed, rodents represent some of the few mammalian species without detectable peak of expression at this developmental stage in the fetal XX gonad i.e. before meiosis. Thus, thanks to the TALEN methodology already shown to be efficient for gene targeting in the rabbit species (Lee *et al.* 2018; Peyny *et al.* 2020), we produced *CYP19A1*

66 knocked-out (KO) rabbits completely devoid of estrogens secretion. Here we report the
67 phenotype of the XX *CYP19A1* KO (*ARO*$^{-/-}$) female rabbits, which are completely infertile at
68 adulthood due to ovarian developmental defects detectable as soon as the first stages of their
69 differentiation.
70
71 **Results**
72 **Three aromatase mutant rabbit lines which do not produce estradiol were generated.**
73 The TALEN subunits were designed to generate *InDel* mutations through non-homologous end
74 joining near the initiation site of translation of the *CYP19A1* gene as described in Figure 1.
75 After transferring 67 injected embryos in 3 recipient female rabbits, 6 founders (2 males and
76 4 females) harboring mutant alleles were characterized from 11 neonates. Each founder F0
77 was mated with a wild type counterpart in order to transmit a mutant allele to the
78 descendants and generate mutant lines carrying one mutated allele per line.
79 Three mutant lines harboring each one a specific mutant allele were generated and studied.
80 Homozygous (*ARO*$^{-/-}$) rabbits were generated by crossing heterozygous (*ARO*$^{+/-}$) rabbits.
81 Mating was performed between rabbits within each line in order to avoid mixing the various
82 mutant alleles.
83 Mutations are shown in Figure 1. A 339, 498 or 829 nucleotide-long (nt) deletion was observed
84 in each of the alleles respectively named Δ339, Δ498 and Δ829. Insertion of a small number
85 of nucleotides was also detected in Δ339 and Δ498 alleles. Briefly, mutations Δ339 and Δ498
86 eliminated the 3' end of exon II including the translation initiation site (ATG codon) plus a large
87 part of the second intron; the mutation Δ829 eliminated a larger fragment encompassing the
88 proximal promoter upstream of exon II, the whole exon II and a large part of the second intron.
89 Thus, in the absence of the translation initiation site, no protein was expected to be translated
90 from any of these mutant alleles. Moreover, the deletion of the 3' part of the exon II
91 theoretically should lead to the elimination of 48 amino acids in the N-terminus of the
92 AROMATASE enzyme. As previously published (Kaur and Bose 2014), these amino acids
93 encompass the signal anchor responsible for the translocation of the protein to the
94 endoplasmic reticulum. It is thus expected that if a protein is translated from the mutant
95 mRNA, it has a good chance to be not correctly embedded in the endoplasmic reticulum
96 bilayer, and consequently not functional.
97

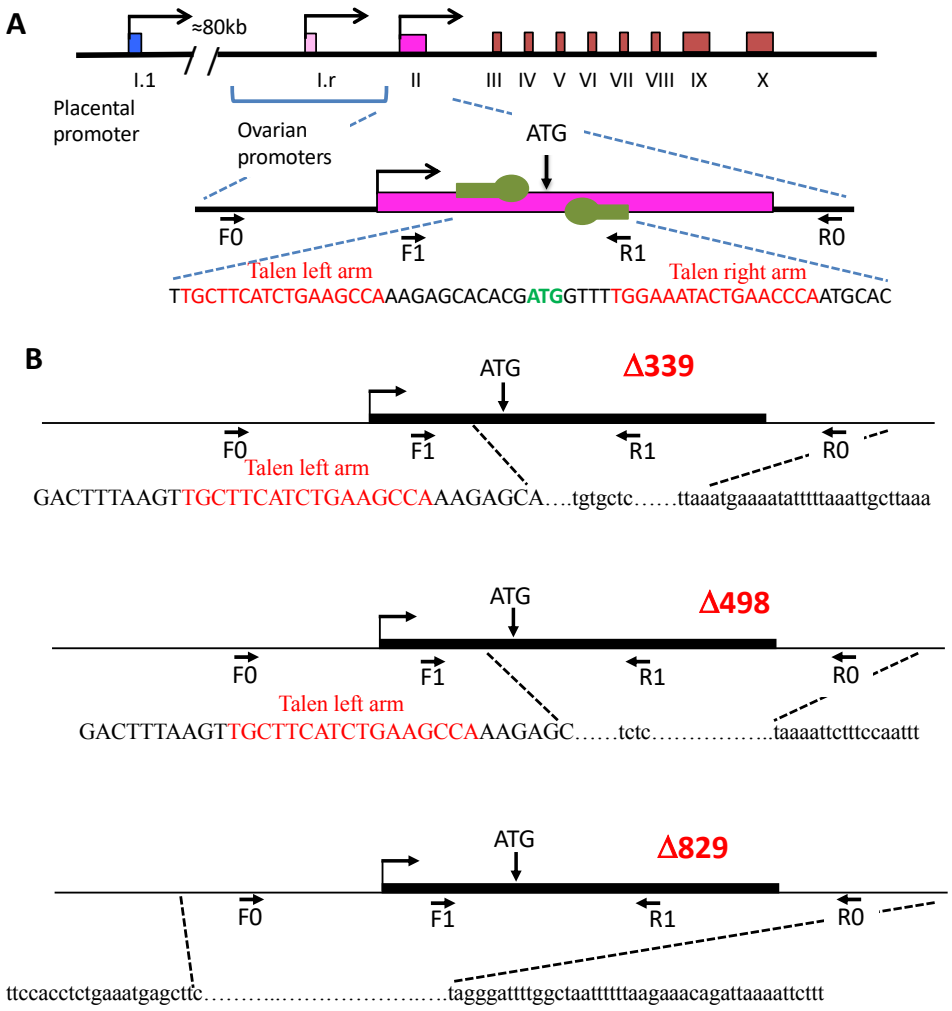

Figure 1: TALEN induced indel mutations in the rabbit *CYP19A1* gene. (A): structure of the rabbit aromatase gene; **(B):** sequences of the mutant alleles Δ339, Δ498 and Δ829

Figure 1: TALEN induced indel mutations in the rabbit *CYP19A1* gene.

(A): structure of the rabbit aromatase gene, with the various tissue specific promoters i.e. the I.1 placental promoter at around 80kb upstream of the transcription start point (tsp, marked by squared arrows) and the two proximal ovarian promoters I.r and II as previously described (Bouraïma *et al.* 2001). The enlargement shows the sequence of the exon II with the initiation site of translation (ATG in green letters). The two subunits (left and right arm) of the TALEN are shown as green symbols and the targeted sequence is written in red. The horizontal black arrows point the primers used for PCR detection of mutants in founders (F0/R0 set) and for routine qPCR genotyping (F1/R1 set).

(B): sequences of the mutant alleles Δ339, Δ498 and Δ829. Capital letters report to exon sequence, lowercase letters to intron sequence. The deletion spans over 339 nucleotides (nt) in the Δ339 mutant allele (149 nt in the 3' end of exon II and 190 nt of intron 2) and over 498 nt in the Δ498 mutant allele (148 nt in the 3' end of exon II and 350 nt of intron 2), both with insertion of few nt at the repair position. In the Δ829 allele, the mutation consisted in the elimination of 829 nt encompassing 250 nt upstream of the beginning of exon II (transcription

112 start site of the gene as regard to the ovarian promoter), the totality of the second exon (263 nt) and 316 nt in
113 the second intron. All mutations suppressed the ATG codon and the splice donor site at the 3' extremity of exon
114 II.
115
116 Finally, to confirm the absence of any active AROMATASE enzyme, we searched for estradiol
117 by Gas Chromatography / Mass Spectrometry (GC/MS) in rabbit serum samples collected after
118 birth and in fetal gonads. The concentrations of estradiol in sera from *ARO*$^{-/-}$ XX females after
119 birth were under the limit of quantification (LOQ = 0,2pg/ml) whatever the age of the animals,
120 when in wild type (*ARO*$^{+/+}$) and heterozygous (*ARO*$^{+/-}$) females the estradiol concentration
121 increased progressively with the age of the animal (supplementary Figure 1). The
122 concentration of testosterone was measured in the same samples. In *ARO*$^{-/-}$ sera, the values
123 ranged in similar way than in WT or *ARO*$^{+/-}$ XX rabbits.
124 We measured also by GC/MS the steroid content of the gonads in fetuses aged of 28 days *post*
125 *coitum* (d*pc*). The estradiol content was undetectable in gonads from all *ARO*$^{-/-}$ XX fetuses and
126 in all XY gonads, when it was always detected, even sometimes in very low amounts, in XX
127 gonads from *ARO*$^{+/-}$ and WT genotypes (supplementary figure 2). Testosterone was not
128 detected in any XX gonads whatever their genotype at the *CYP19A1* locus. This shows that
129 androgens were not over-synthesized nor accumulated in XX *ARO*$^{-/-}$ gonads. Finally, these data
130 also show that neither estradiol nor testosterone from maternal or placental origin was
131 detected in the 28d*pc* fetal gonads.
132
133 **XY and XX *ARO*$^{+/-}$ rabbits were fertile, with normal genital tracts and normal gonads**
134 **morphology**
135 In the three mutant lines, all *ARO*$^{+/-}$ and XY *ARO*$^{-/-}$ rabbits were viable until adults and did not
136 suffer apparently from any metabolic or postural disease at least until 2 years after birth. No
137 apparent modification of external genitalia was visible. All were fertile and gave birth to
138 progeny. The sexual behavior was not studied. The number of neonates per litter from
139 heterozygous mating (♀*ARO*$^{+/-}$ x ♂*ARO*$^{+/-}$) was similar to that of wild type mating (♀WT x
140 ♂WT) (supplementary Figure 3). The percentage of mating without pregnancy was not
141 different: 37,9% (11 null per 29 mating) in WT x WT mating and 35,3% (23 null per 65 mating)
142 in heterozygous x heterozygous mating. All this suggests that the fertility of heterozygous
143 animals was not affected.

144 At puberty (5-6 months after birth), genital tracts and gonads were not different in
145 heterozygous and wild type XX rabbits (supplementary Figure 4). Since all measured
146 parameters did not differ in heterozygous and wild type females (similar estradiol and
147 testosterone serum levels, similar prolificacy, similar overall structure of genital tracts and
148 ovaries), we used ovary samples indifferently from wild type or heterozygous females as
149 reference ones. Nevertheless, the genotype has always been distinctly reported in the legends
150 of all figures.
151
152 **XX *ARO*$^{-/-}$ rabbits developed small female genital tracts, ovaries with almost no follicular**
153 **reserve and very few antral follicles.**
154 All XX *ARO*$^{-/-}$ rabbits were viable without any metabolic or postural disease at least until 1.5
155 years after birth. No apparent modification of external genitalia was visible. The sexual
156 behavior of XX *ARO*$^{-/-}$ rabbits was not studied in detail.
157 Obvious modifications of the genital tracts and ovaries were observed in XX *ARO*$^{-/-}$ rabbits
158 from the three lines with similar characteristics. After puberty, a typical phenotype was
159 observed, with under-developed uterus horns, oviducts and pavilions resembling those of
160 neonatal females. Their size was clearly smaller than in wild type or heterozygous females
161 (supplementary Figure 4). In all three lines, XX *ARO*$^{-/-}$ gonads developed like ovaries (Figure 2,
162 supplementary Figure 5) but with a very small size. As the phenotype was identical in Δ339,
163 Δ498, and Δ829 lines, it is hardly attributable to any off-target alteration of the genome.
164 Ovaries contained almost no primordial follicles, scarce primary and secondary follicles, and
165 were filled with numerous remnants of atretic follicles. The abundant follicle reserve
166 composed of primordial follicles observed at the cortex of wild type ovaries (Figure 2A and B)
167 was absent in *ARO*$^{-/-}$ gonad mutants (Figure 2C and D). Nevertheless, some follicles developed
168 to reach the large antrum stage in *ARO*$^{-/-}$ ovaries, showing granulosa and theca cell layers,
169 oocyte and cumulus. The number of large antrum follicles was high in some females (see the
170 ovary of the Δ829 female in supplementary Figure 5) possibly reflecting the surge of
171 gonadropins that occurs at early puberty (around 5-6 months in the rabbit). Numerous Call-
172 Exner bodies (spherical deposits of basal lamina matrix surrounded by granulosa cells,
173 observed in rabbits and some mammals) were observed in the granulosa of growing follicles
174 in *ARO*$^{-/-}$ ovaries as classically observed in wild type ones (Lee et al. 1996). The number of
175 pyknotic cells or of cells with dense colored nuclei was low.

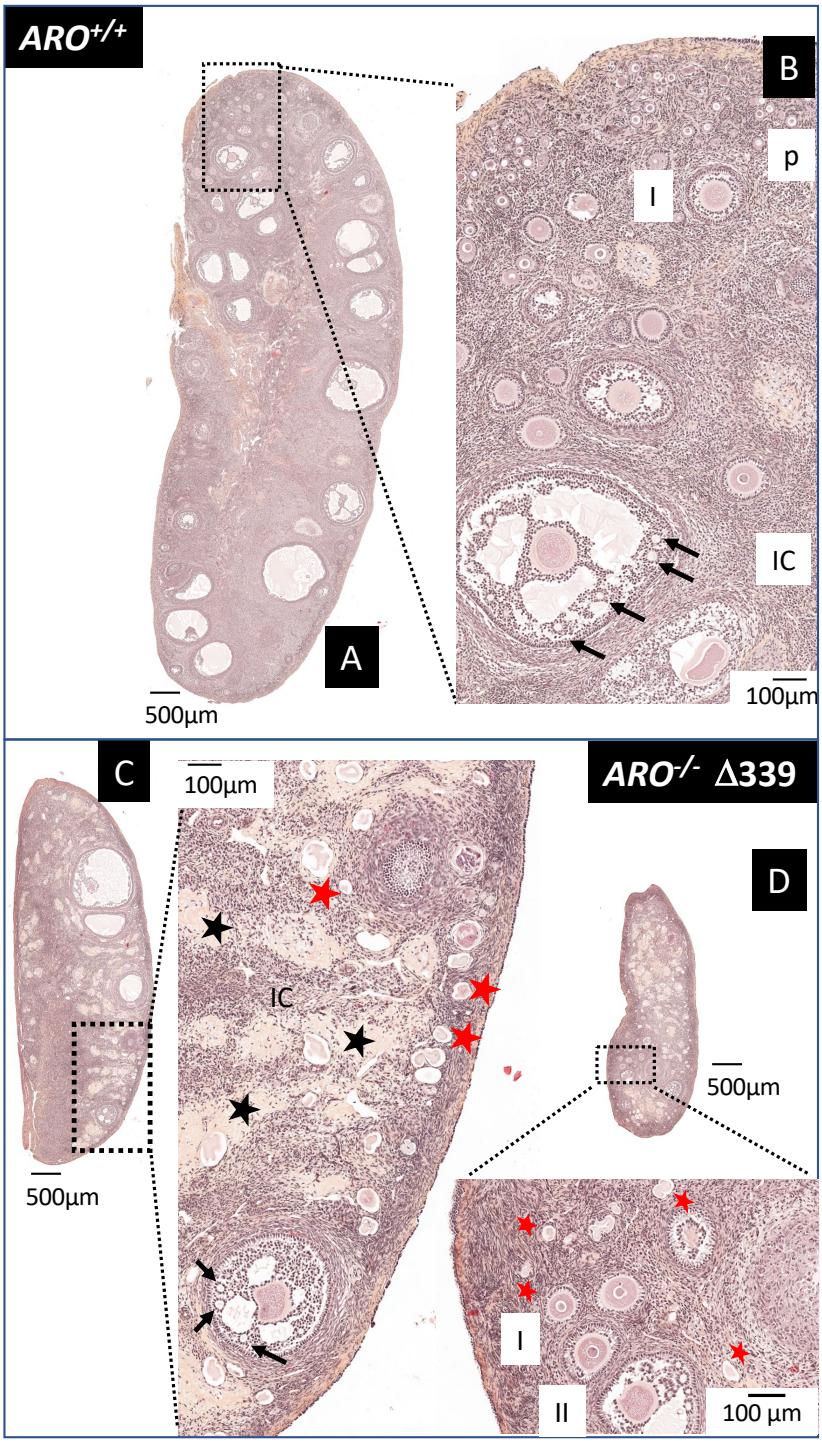

Figure 2: ovaries of adult *ARO*$^{-/-}$ rabbits were small with few follicles and filled with collagen rich connective tissue. Ovaries from wild type female rabbits (*ARO*$^{+/+}$, A and B) and from the mutant *ARO*$^{-/-}$ line Δ339 (C and D) were fixed in PAF then HES colored. Females were 5,5 months old.

Figure 2: ovaries of adult *ARO*$^{-/-}$ rabbits were small with few follicles and filled with collagen rich connective tissue.

Ovaries from wild type female rabbits (*ARO*$^{+/+}$, A and B) and from the mutant *ARO*$^{-/-}$ line Δ339 (C and D) were fixed in PAF then HES colored. Females were 5,5 months old. Two distinct sections of the same ovary are presented for the mutant *ARO*$^{-/-}$ to show the follicles that were otherwise not visible. Enlarged zones point the

182 different types of follicles. Black arrows = Call-Exner bodies. Black stars = accumulation of fibrous tissue. Red
183 stars = remnants of degenerated follicles. “p” = primordial follicle; I = primary follicle; II = secondary follicle; IC =
184 interstitial cells. The phenotype of the *ARO*$^{-/-}$ ovary was similar in the other lines Δ498 and Δ829 (supplementary
185 Figure 5).
186
187 The expression of the marker genes *RSPO2* and *FOXL2* specific respectively for the oocyte and
188 for the granulosa cells in differentiating follicles was studied by *in situ* hybridization (ISH,
189 Figure 3). In the *ARO*$^{-/-}$ ovary, the rare detected oocytes were positive for the *RSPO2* labelling
190 (Figure 3A), and granulosa cells were positive for *FOXL2* (Figure 3B). In wild type ovaries,
191 AROMATASE was immuno-detected in a small number of follicles with antrum, thus
192 characterizing the pre-ovulatory ones (Figure 3C). The Anti Müllerian Hormone (AMH) was
193 immuno-detected in granulosa cells of many follicles in wild type ovaries except those positive
194 for AROMATASE. In *ARO*$^{-/-}$ ovaries, granulosa cells of all follicles were AROMATASE negative
195 and AMH positive (Figure 3D). However, the AMH serum level was lower in *ARO*$^{-/-}$ females,
196 reflecting the small number of follicles and/or their poor synthesis capacity.

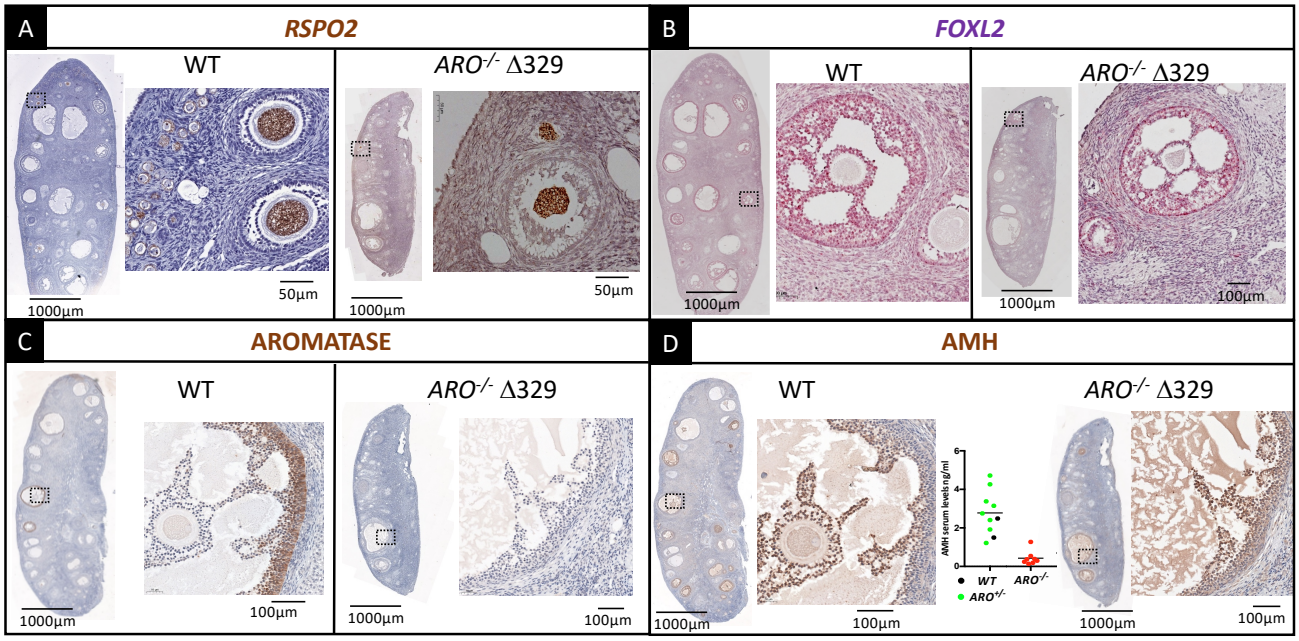

Figure 3: *RSPO2, FOXL2* and AMH were detected in wild type and ARO$^{-/-}$ adult ovaries. In Situ Hybridization to localize mRNA of *RSPO2* and *FOXL2* genes and immunodetection of AROMATASE and AMH in adult ovaries. Ovaries were collected in wild type (WT) or *ARO*$^{-/-}$ Δ329 females aged 5-6 months.

197
198 **Figure 3: *RSPO2, FOXL2* and AMH were detected in wild type and ARO$^{-/-}$ adult ovaries.** In Situ Hybridization to
199 localize mRNA of *RSPO2* and *FOXL2* genes and immunodetection of AROMATASE and AMH in adult ovaries.
200 Ovaries were collected in wild type (WT) or *ARO*$^{-/-}$ Δ329 females aged 5-6 months. The expression of *RSPO2* (A)
201 and *FOXL2* (B) genes was detected by ISH probes. AROMATASE (C) and AMH (D) were detected by
202 immunohistochemistry on two adjacent sections. The *RSPO2* and *FOXL2* probes labelled respectively the

203 cytoplasm of oocytes (brown dots) and of granulosa cells (red dots) from all follicles, from primordial to antrum
204 stages in wild type and *ARO*$^{-/-}$ rabbits as well. Some thecal cells were also positive for the *FOXL2* labelling in both
205 genotypes. Mural granulosa cells from pre-ovulatory follicles were positively labelled by the anti-AROMATASE
206 antibody in wild type ovaries (brown colored); no cells were positive in *ARO*$^{-/-}$ ovaries. The anti-AMH antibody
207 labelled most granulosa cells of growing follicles in wild type ovaries (brown colored), excepted those positive
208 for AROMATASE. In *ARO*$^{-/-}$ ovaries, all follicles with antrum were positively labelled. Similar staining were
209 observed in females from the two other strains. The graph represents the AMH serum level in *WT* (black points),
210 *ARO*$^{+/-}$ (green points) and *ARO*$^{-/-}$ (red points) females.
211
212 Intense modifications affected the medulla of the ovary. In wild type rabbits, the medulla
213 consisted mostly in interstitial tissue composed of cells with large clear cytoplasm and round
214 regular shape nuclei (Figure 2B); besides, in *ARO*$^{-/-}$ ovary, the interstitial tissue appeared as a
215 mixture of cells with heterogeneous shape and angular nuclei. More, several areas filled with
216 fibrous material rich in collagen and devoid of cells were detected (Figure 2C and D;
217 supplementary Figure 5).
218 Some of the heterozygous (*ARO*$^{+/-}$) and homozygous (*ARO*$^{-/-}$) 10 months old XX rabbits were
219 hormonally treated to induce ovulation, mated and sacrificed to collect gonads for histological
220 analysis. Ovulation rupture points were observed in ovaries from *ARO*$^{+/-}$ rabbits, but not in
221 *ARO*$^{-/-}$ ovaries (supplementary Figure 6). While several primordial, primary, pre-antral and
222 antral follicles were detected at the cortical periphery of ovaries in *ARO*$^{+/-}$ rabbits after super-
223 ovulation treatment, no primordial or primary follicles were seen in the treated *ARO*$^{-/-}$ ovarian
224 cortex. Nevertheless, some large antrum type follicles were observed in *ARO*$^{-/-}$ ovaries, with
225 developed granulosa, theca cells, and oocyte.
226
227 **The mutation impacted the XX gonad from the first stages of their differentiation**
228 Our goal was to search when and how ovaries were impacted by the lack of functional
229 AROMATASE enzyme and of estradiol during fetal life. In the rabbit species, pregnancy spans
230 for 31 days. The present study analyzed the fetal gonads from 18 d*pc* onwards. At this stage
231 in rabbits, the gonadic sex is already determined, the multiplication of germ cells and somatic
232 cells is intense (Chretien 1966) and the peak of *CYP19A1* gene expression starts in the ovary,
233 concomitantly with the increase of *FOXL2* gene expression (Daniel-Carlier *et al.* 2013). At 20
234 d*pc*, we detected a specific labelling with a *CYP19A1* ISH probe in cells of the surface
235 epithelium and cells forming invaginated structures issued from this epithelium

236 (supplementary Figure 7). Simultaneously, we observed that these same cells were labelled
237 by an *ESR1* specific ISH probe and we detected a surge of the expression of the estrogen
238 receptor alpha gene (*ESR1*) by RT-qPCR (supplementary Figure 7). The *FOXL2* gene was mainly
239 expressed in somatic cells underneath the surface epithelium and those surrounding
240 invaginated structures (ISH labelling, supplementary Figure 7). Only few cells of the surface
241 epithelium were clearly positive for both the *CYP19A1* and *FOXL2* ISH probes. The expression
242 of the *ESR2* gene coding for the estrogen receptor beta was low at these stages compared
243 with the levels determined later at birth (34 d*pc*). In agreement, a faint labelling was observed
244 by ISH labelling (supplementary Figure 7).
245 Therefore, the morphology of the gonads and the location of specific markers were
246 investigated at various fetal stages and compared between wild type or heterozygous gonads
247 *versus* $ARO^{-/-}$ ones from the stage of gonadal determination onwards. At 18 d*pc*, the gonads
248 from all XX fetuses, $ARO^{-/-}$ and $ARO^{+/-}$, were differentiated as ovaries with the same
249 morphology except a thinner coelomic epithelium in $ARO^{-/-}$ gonads (Figure 4A). Regardless of
250 the developmental stages, XX $ARO^{-/-}$ gonads showed no evidence of testicular appearance (see
251 for comparison the 18 d*pc* testis in the supplementary Figure 8). A similar density of OCT4
252 positive germ cells was detected in $ARO^{-/-}$ and $ARO^{+/-}$ gonads, as shown by the labelling with
253 specific antibodies directed against OCT4 (Figure 4B). Mitotic activity was detected by KI67
254 immunostaining (Figure 4C). KI67 positive cells were mainly present in the ovarian surface
255 facing the abdominal cavity and in invaginated structures below in both $ARO^{+/-}$ and $ARO^{-/-}$
256 ovaries. Interestingly, the KI67-positive ovarian surface appeared thinner in KO gonads than
257 in the $ARO^{+/-}$ controls (Figure 4C).
258

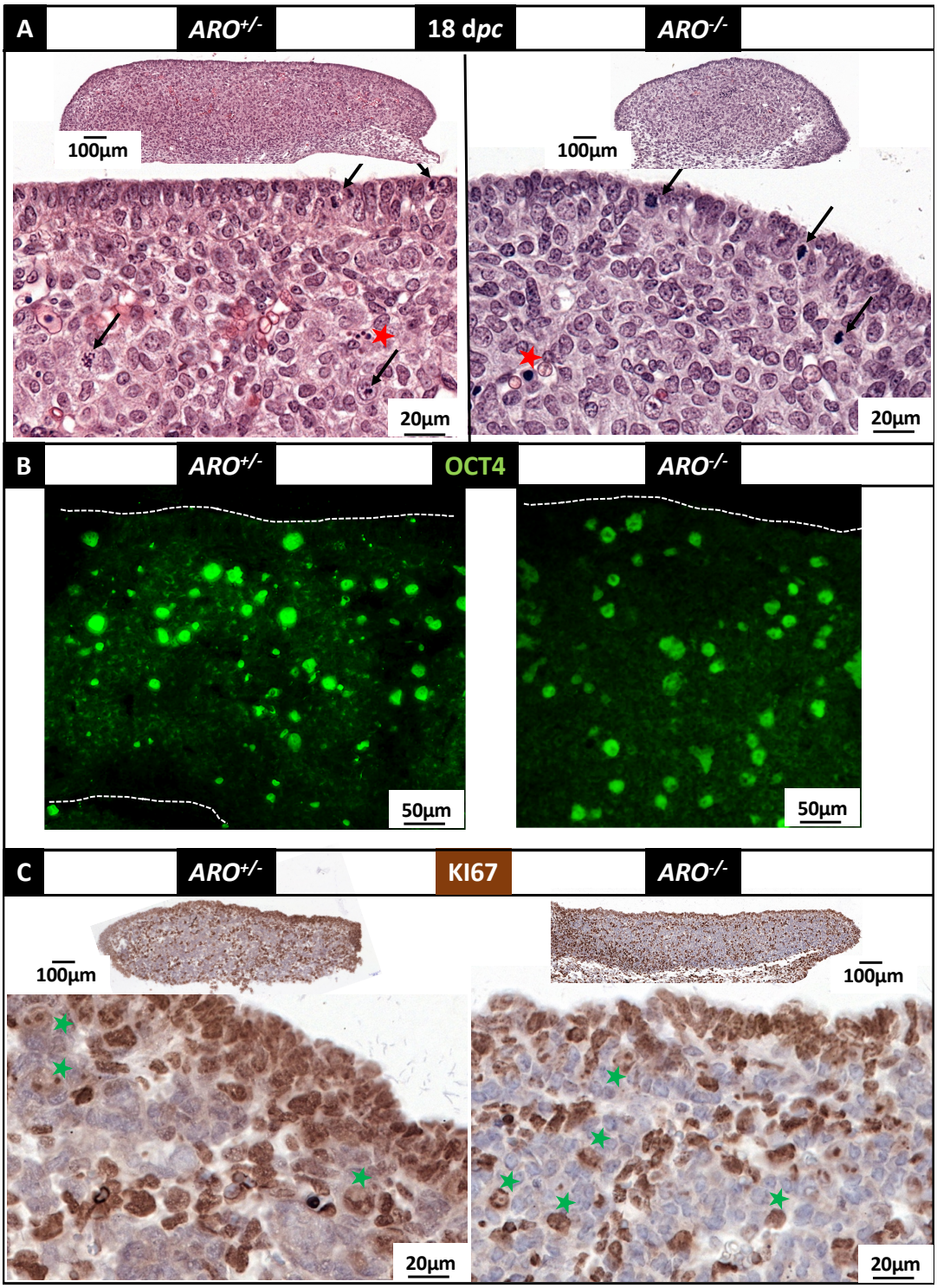

Figure 4: morphology and detection of OCT4 and KI67 in ovaries from *ARO*$^{+/-}$ and *ARO*$^{-/-}$ 18 d*pc* old fetuses.

Figure 4: morphology and detection of OCT4 and KI67 in ovaries from *ARO*$^{+/-}$ and *ARO*$^{-/-}$ 18 d*pc* old fetuses. Gonads were collected at 18 d*pc* in *ARO*$^{+/-}$ and *ARO*$^{-/-}$ fetuses, fixed in Bouin's then HES colored (A) or fixed in PAF then treated for antibody labelling (B and C). **(A): HES coloration**. The surface epithelium appeared as a continuous layer of epithelial cells. Red stars point dense nuclei that could correspond to pyknotic nuclei. Arrows point figures of mitoses. **(B): detection of OCT4 positive cells.** The immune-labelling was visualized using a

265 fluorescent secondary antibody. Nuclei of positive cells (large round green-labelled) were dispersed through the
266 gonad in both *ARO*$^{+/-}$ and *ARO*$^{-/-}$ ovaries. **(C): detection of KI67 positive cells.** The immune-labelling was visualized
267 using a peroxidase coupled secondary antibody. Positive cells with brown colored nuclei were found at the
268 surface epithelium, and in rows of cells delimiting cell clusters. Green stars point brown light-colored large nuclei,
269 possibly corresponding to germ cells.
270
271 From 20 d*pc* onwards, more important alterations progressively appeared in *ARO*$^{-/-}$ ovaries.
272 The cortex was thinner, composed of a single layer of epithelial cells, connected to small size
273 nascent ovigerous cords, by opposition to the thick cortex observed in *ARO*$^{+/-}$ ovaries,
274 connected to numerous large size ovigerous cords (Figure 5A and 5D). A discontinuous layer
275 of cells with small and dense colored nuclei was observed underneath the surface epithelium,
276 forming at 22 d*pc* (Figure 5D) and later on (34 d*pc*, Figure 9) a loose connective tissue between
277 the thin cortex and the inside of the ovary.
278 The cells of the surface epithelium expressed the *ESR1* gene in both genotypes (Figures 5B and
279 5E). The intensity of the ISH *ESR1* labelling varied greatly at the surface of the *ARO*$^{+/-}$ ovaries
280 as shown in figure 5 (compare 5B, E, C and F, which are different sections from the same
281 gonad). Nevertheless, in all treated sections, clusters of labelled *ESR1* cells connected to the
282 surface epithelium were easily observed. Besides, in *ARO*$^{-/-}$ ovaries, labelled *ESR1* cells were
283 mainly dispersed in the inner of the gonad. Similarly, the *FOXL2* ISH probe labelled evenly
284 dispersed cells in the inner of the *ARO*$^{-/-}$ gonad, which differed from the strong *FOXL2* labelled
285 cell cords of the *ARO*$^{+/-}$ ovary. *OCT4* positive germ cells were detected in both genotypes but
286 the hybridization signals were lighter in *ARO*$^{-/-}$ germ cells (Figures 5C and 5F-H). Numerous
287 were found in the surface epithelium, interestingly in close contact with somatic cells
288 expressing the *ESR1* gene.
289

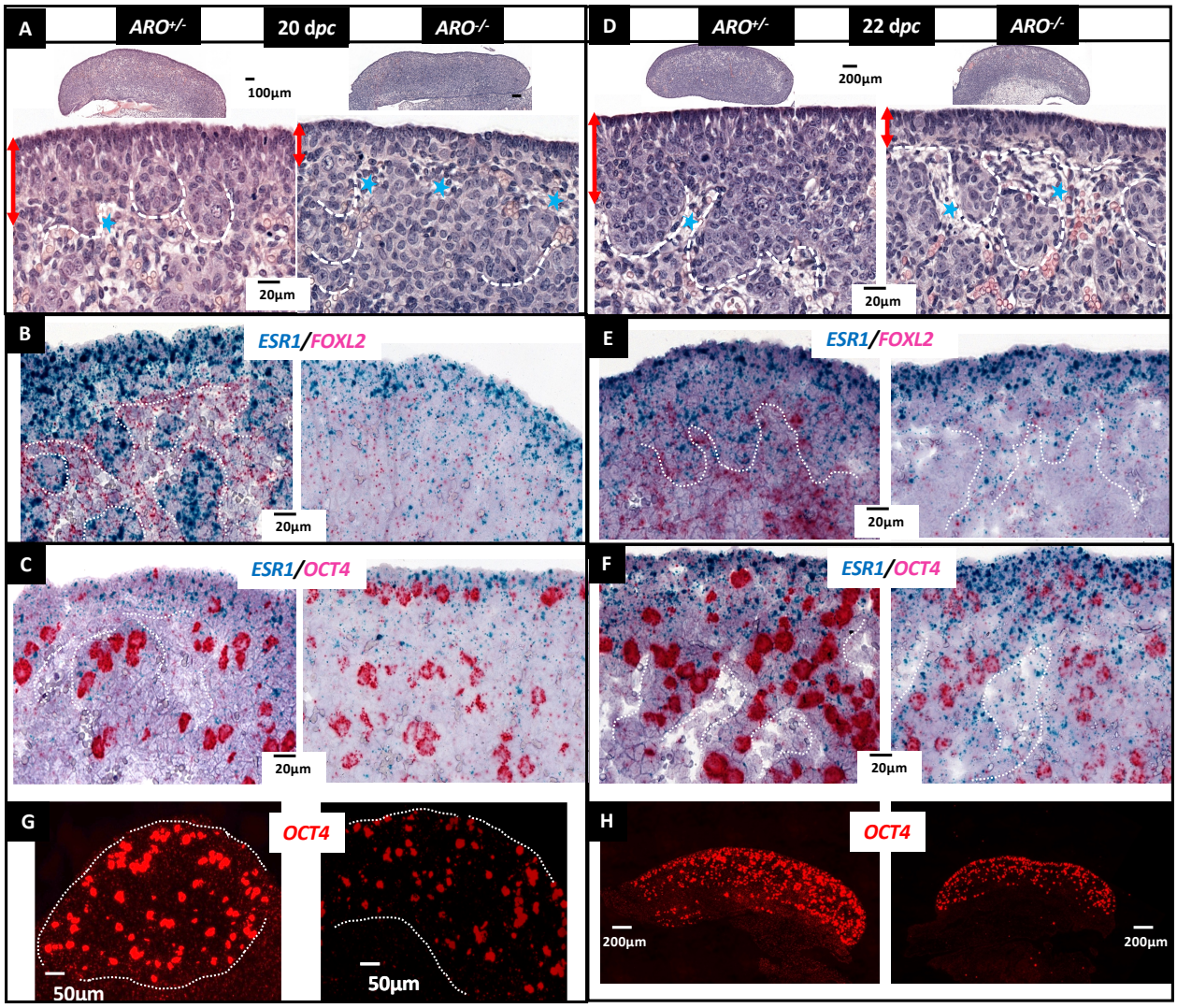

Figure 5: gradual modifications of *ARO*$^{-/-}$ ovaries at 20 and 22 d*pc*. *ESR1*, *FOXL2* and *OCT4* gene expressions were labelled by dual HIS.

Figure 5: gradual modifications of *ARO*$^{-/-}$ ovaries at 20 and 22 d*pc*.

Gonads were collected from *ARO*$^{+/-}$ and *ARO*$^{-/-}$ fetuses, fixed in Bouin's then HES colored **(A, D).** Ovigerous nests and cords are underlined by a dotted white line in **A-F**. The red double arrow points the thickness of the nascent cortex. Blue stars point the connective tissue. In situ hybridization was performed to visualize simultaneously two RNA targets to show the *ESR1* (blue points) and *FOXL2* (fast red points) RNAs **(B, E)**, and the *ESR1* (blue) and *OCT4* (fast red) RNAs **(C, F)**. The lower panel is the fluorescence observation of the fast red *OCT4* ISH labelling to show the overall density of the *OCT4* positive cells (**G, H**).

KI67 positive cells were overall detected in both types of ovaries at 22 d*pc* (Figure 6A) but there was still a clear difference of mitotic activity in the coelomic epithelium between *ARO*$^{+/-}$ and *ARO*$^{-/-}$ ovaries. Indeed, while many KI67 positive cell layers were detected in the coelomic epithelium of *ARO*$^{+/-}$ gonads, only one layer was visible in the *ARO*$^{-/-}$ one. The γH2AX-antibody, marker of double strand breaks of the DNA, labelled mostly germ cells in both types of ovaries

304 as suggested by their large round nuclei (Figure 6B). The density of γH2AX positive cells
305 (probably apoptotic cells) was apparently not different in *ARO*$^{+/-}$ and *ARO*$^{-/-}$ ovaries.

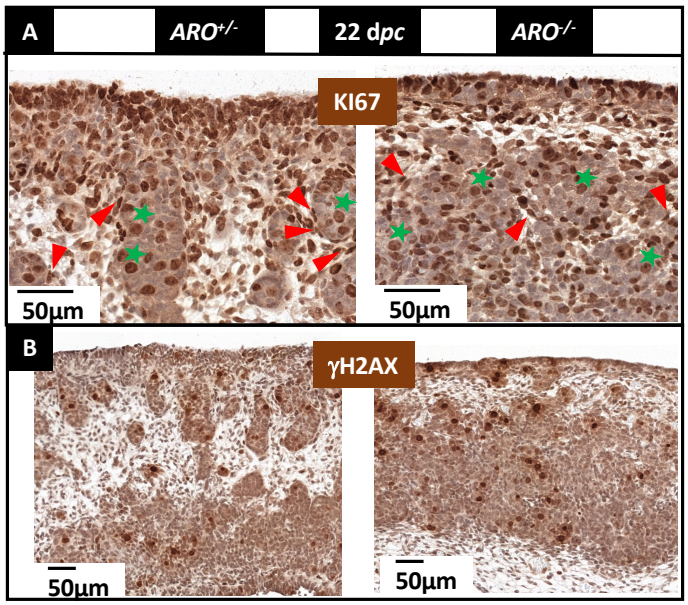

Figure 6: mitotic activity and DNA fragmentation at 22 d*pc*.
The marker of mitotic activity KI67 **(A)**, and that of double strand breaks gH2AX **(B)** were localized by immunohistochemistry in sections from PAF fixed ovaries of *ARO*$^{+/-}$ and *ARO*$^{-/-}$ fetuses at 22 d*pc*.

306

307 **Figure 6: mitotic activity and DNA fragmentation at 22 d*pc*.**
308 The marker of mitotic activity KI67 **(A)**, and that of double strand breaks γH2AX **(B)** were localized by
309 immunohistochemistry in sections from PAF fixed ovaries of *ARO*$^{+/-}$ and *ARO*$^{-/-}$ fetuses at 22 d*pc*. The KI67
310 antibody labelled nuclei of most cells of the coelomic epithelium, and numbers of cells inside the ovary in both
311 genotypes. Cells with flat nuclei KI67 positive (red arrowheads) surrounded from place to place the ovigerous
312 cords. Cells with large round nuclei positive for KI67 labelling (probably germ cells) were found mainly at the
313 inside of the cords (green stars). The γH2AX antibody labelled large round shape nuclei corresponding probably
314 to germ cells. Note the disconnection between the coelomic epithelium and the new forming ovigerous cords in
315 *ARO*$^{-/-}$ ovaries.
316
317 The relative expression levels of key marker genes were determined at these developmental
318 stages on total RNAs extracted from the whole gonads (Figure 7). The expression levels of the
319 *OCT4* and *FOXL2* genes were reduced in *ARO*$^{-/-}$ ovaries, reflecting a reduction of the number
320 of *OCT4* positive germ cells and *FOXL2* positive somatic cells respectively. Interestingly, the
321 expression level of the *DDX4* gene, known to be its lowest at this ovarian developmental stage
322 (Daniel-Carlier *et al.* 2013), did not differ between WT and *ARO*$^{-/-}$. It increased between 20 and
323 22 d*pc*, which reflects the early differentiation of germ cells from the pluripotent stage. The

324 *SOX9* gene expression level was 5- to 10 times lower in the ovaries from all genotypes than in
325 testes at the same age. The *SOX9* gene was not detected by immunohistology either in wild
326 type or in *ARO*$^{-/-}$ ovaries, while a clear labeling was observed in the fetal testis at 22 d*pc*
327 (supplementary Figure 8). This reinforces the demonstration that *ARO*$^{-/-}$ ovaries did not show
328 any sex-reversal phenotype. The expression levels of the *ESR1* and *ESR2* genes did not change
329 significantly.

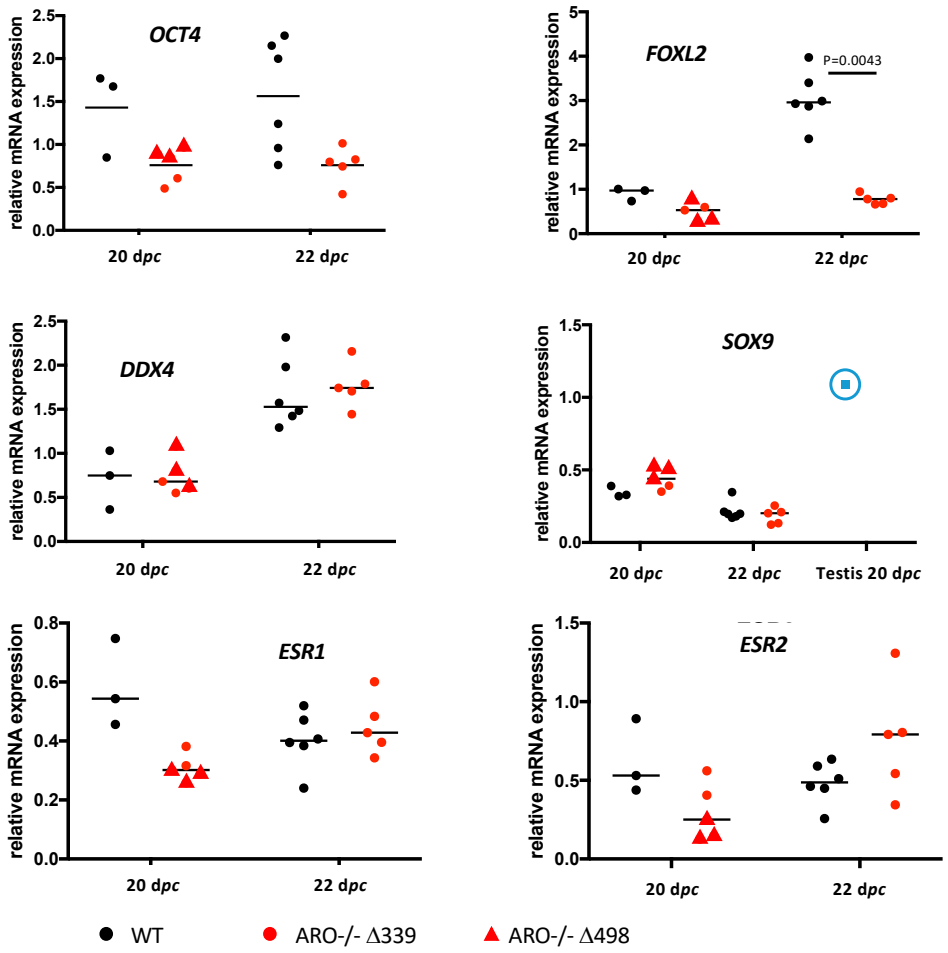

Figure 7: gene expression in 20 and 22 d*pc* ovaries from WT and *ARO*$^{-/-}$ fetuses.
Ovaries were collected from wild type and mutant fetuses. The diagrams show the relative mRNA expression levels.

330

331 **Figure 7: gene expression in 20 and 22 d*pc* ovaries from WT and *ARO*$^{-/-}$ fetuses.**
332 Ovaries were collected from wild type and mutant fetuses. The diagrams show the relative mRNA expression
333 levels. Each point represents one RNA sample extracted from both gonads of one animal at the indicated
334 developmental stage. The same RNA samples were analyzed in the 6 diagrams. Red triangles refer to mutant
335 from Δ339 line, and red point from Δ829 line. No samples from line Δ498 were analyzed. The blue point in the
336 *SOX9* diagram shows the *SOX9* mRNA level measured in the two testes of one 20 d*pc* WT fetus. Horizontal bars
337 represent the medians. At these stages *DDX4* and *ESR2* gene expression levels were very low, but significantly
338 measured.

339

340 Thus, from 20 d*pc* onwards, the differentiation of the *ARO*$^{-/-}$ gonad was profoundly modified,
341 with a decrease of proliferation of the somatic cells of the coelomic epithelium and a reduction
342 of the number of germ cells. Finally this leads to a clearly underdeveloped small organ with
343 small ovigerous nests, an abnormal distribution and differentiation of the *FOXL2* positive cells
344 and the spread of connective tissue underneath the surface epithelium.

345

346 **Impact of estrogens deprivation on germ cell meiosis and follicular differentiation**

347 In the rabbit ovary, the first signs of meiosis are histologically detected at 30-31 d*pc,* i.e.
348 around birth. Later on, typical meiotic germ cells (prophase I) are observed for less than 2
349 weeks. After meiosis arrest at diplotene stage, follicles begin to differentiate. The peak of
350 expression of the *STRA8* gene that starts at 24-28 d*pc* (Daniel-Carlier *et al.* 2013) marks the
351 commitment of germ cells to meiosis. Thus, we sought to analyze at 28 d*pc* (meiosis
352 commitment), 34 d*pc* (beginning of meiosis) and few days or weeks after birth
353 (folliculogenesis) whether initiation and arrest of meiosis I and early follicular formation were
354 impacted in *ARO*$^{-/-}$ ovaries.

355 In wild type and *ARO*$^{-/-}$ 28 d*pc* ovaries, numerous germ cells were positively labelled by the
356 *OCT4*, *DDX4* and *STRA8* ISH specific probes (Figures 8B, 8C, 8D). The *STRA8* labelling proves
357 the overall commitment of germ cells in meiosis in WT and *ARO*$^{-/-}$ ovaries. However, in these
358 later, the number of positive germ cells for the three probes was low. More, they were
359 clustered in small ovigerous-like structures, while they were all observed in large ovigerous
360 cords in wild type ovaries. Positive *FOXL2* labelled cells were also much less numerous in *ARO*$^{-}$
361 $^{/-}$ ovaries, as shown by the few numbers of hybridization labels. Nevertheless, some of these
362 *FOXL2* positive cells harbored a flattened shape and surrounded the small ovigerous-like
363 structures embedding germ cells, as in wild type ovaries (Figure 8E).

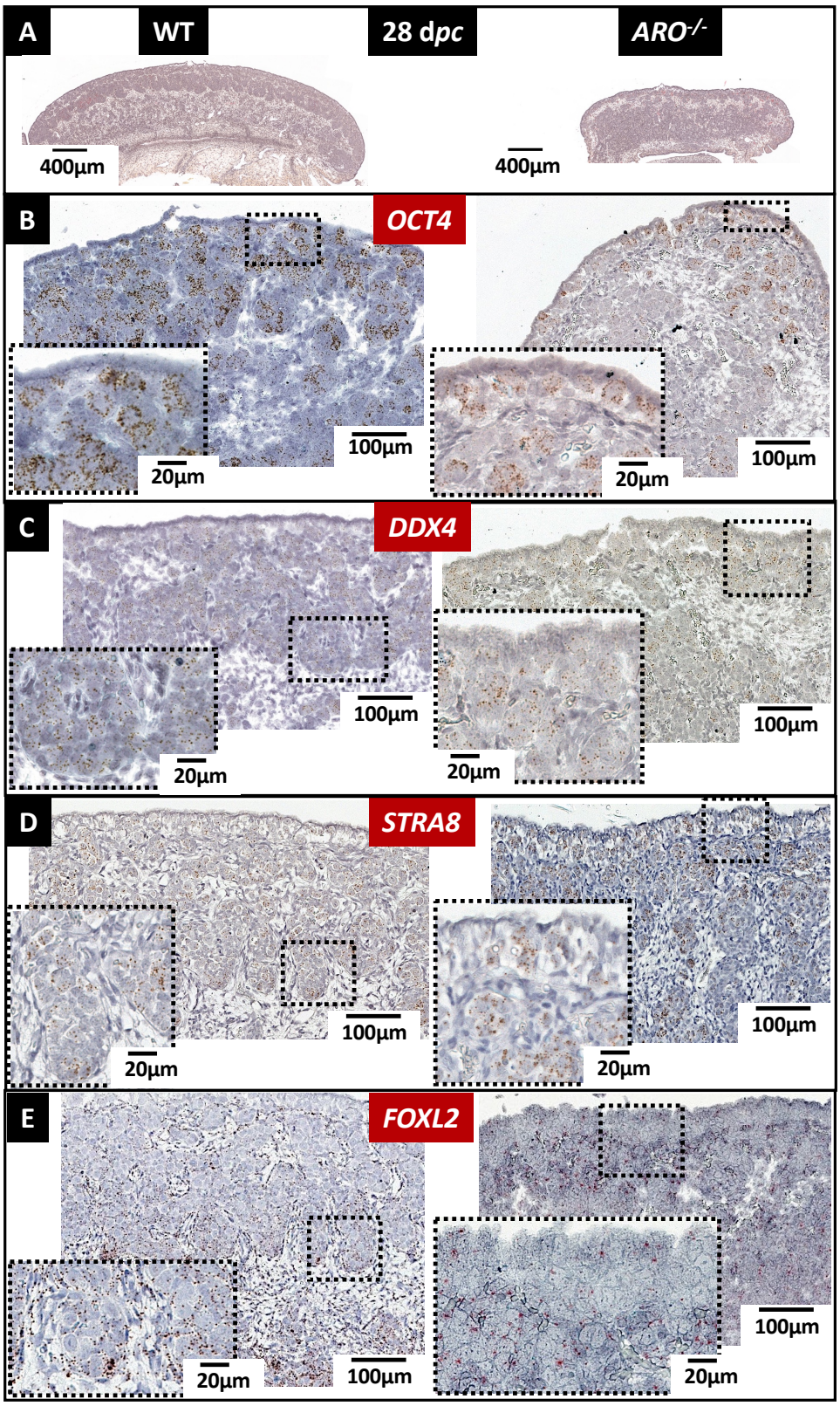

Figure 8: germ cells were committed to meiosis in WT and *ARO*$^{-/-}$ ovaries from 28 d*pc* old fetuses.

Figure 8: germ cells were committed to meiosis in WT and *ARO*$^{-/-}$ ovaries from 28 d*pc* old fetuses.
Ovaries collected at 28 d*pc* were fixed in PAF, then HES colored or analyzed by ISH. **(A): morphology of the ovaries**. The pictures show the difference of the overall size of the gonad and the different thickness of the

368 cortex. The *OCT4* **(B)** and *DDX4* **(C)** ISH probes labelled respectively pluripotent germ cells and differentiating
369 ones. The *STRA8* ISH probe **(D)** labelled germ cells committed to meiosis. The *FOXL2* ISH probe **(E)** labelled the
370 differentiating somatic cells. Note that the latter were mainly distributed around and inside the ovigerous cords
371 in the WT ovaries, and in contrast were dispersed throughout the gonad in the *ARO*$^{-/-}$ rabbit. As in all ISH pictures,
372 positive labeling appears as colored dots.
373
374 At 34 d*pc*, in wild type ovaries, most ovigerous cords were filled with numerous zygotene germ
375 cells, thus showing that meiosis had begun in a majority of germ cells (Figure 9A and a1). In
376 contrast, in the *ARO*$^{-/-}$ ovaries, germ cells at zygotene were sparse (Figure 9B and b1, b2). The
377 differentiation of the *ARO*$^{-/-}$ ovaries was further altered as shown by the low staining observed
378 with *DDX4*, *STRA8, SPO11* and *FOXL2* probes and by the qPCR low expression of these genes
379 (figure 9 C-F). The ratios of the *STRA8/DDX4* and *SPO11/DDX4* mRNA levels were lower in *ARO*$^{-}$
380 $^{/-}$ ovaries, suggesting that germ cells expressing *STRA8* and *SPO11* gene expression, and thus
381 undergoing meiosis, were less abundant in *ARO*$^{-/-}$ ovaries.

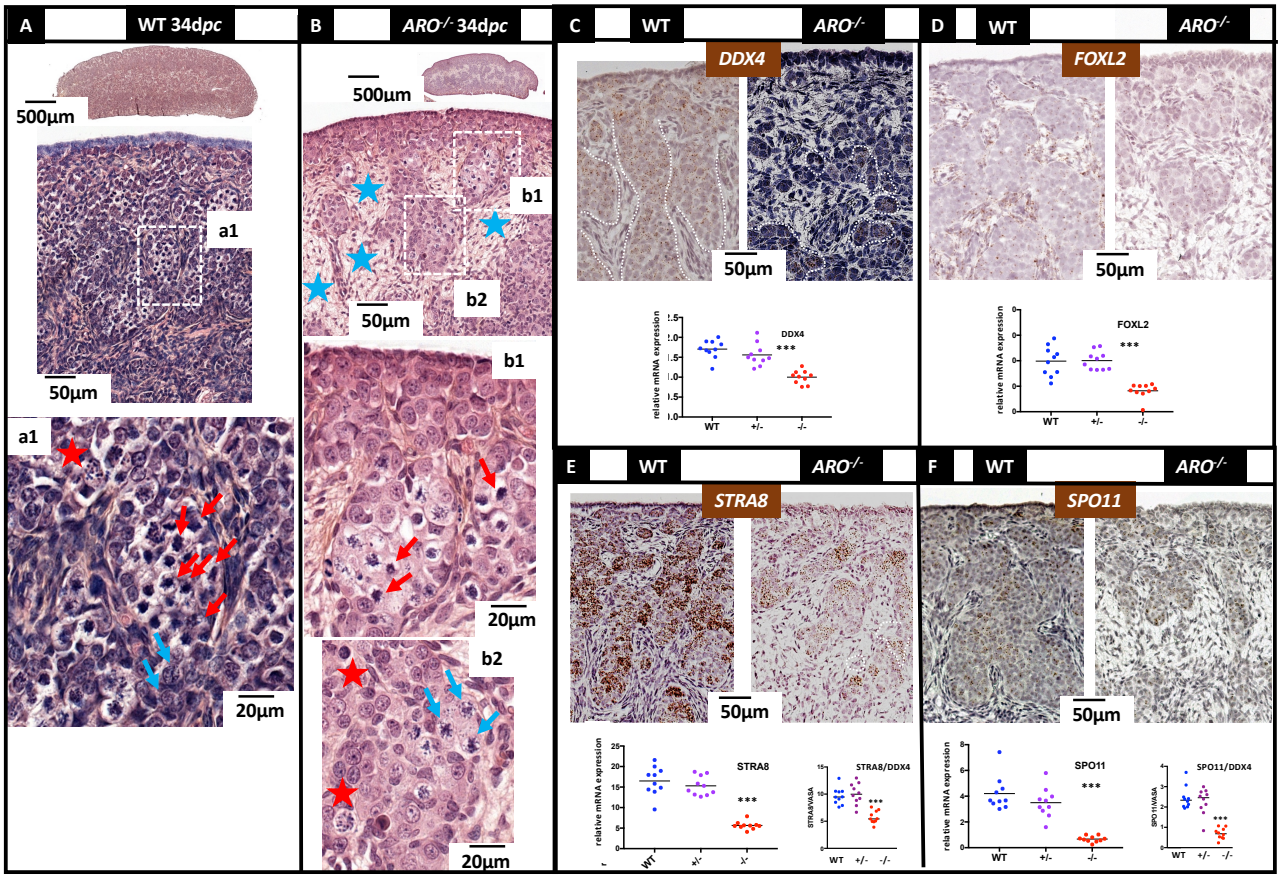

Figure 9: meiosis in WT and *ARO*$^{-/-}$ ovaries. Ovaries were collected at 34 d*pc* (3-4 days after birth)

382
383 **Figure 9: meiosis in WT and *ARO*$^{-/-}$ ovaries.** Ovaries collected at 34 d*pc* (3-4 days after birth) were fixed in Bouin's
384 then HES colored (**A-B**) or PAF then ISH treated (**C-F**). The stages of meiosis were identified as previously
385 published (Peters *et al.* 1965). **(A):** In wild type ovaries, large ovigerous cords were filled with numerous germ

386 cells in zygotene (a1, red arrows). Few pachytene stages were observed at the inner part of the cords (a1, blue
387 arrows). **(B):** In *ARO*$^{-/-}$ ovaries, the rare ovigerous cords were filled with a few numbers of germ cells in zygotene
388 (b1). As in wild type ovaries, some germ cells in pachytene were found at the inner part of the cords (b2). In both
389 ovaries, aberrant pictures of cell nuclei were characterized by punctiform or condensed and dark colored
390 chromatin (red stars). Blue stars show the connective tissue already observed mostly in *ARO*$^{-/-}$ ovaries. **(C-F):** ISH
391 was performed using *DDX4* (**C**), *FOXL2* (**D**), *STRA8* (**E**) and *SPO11* (**F**) genes specific probes. In wild type ovaries,
392 numerous germ cells positive for *DDX4*, *STRA8* and *SPO11* filled the ovigerous cords; pre-granulosa cells *FOXL2*
393 positive were found around and inside the cords. In *ARO*$^{-/-}$ ovaries, germ cells positive for these same ISH probes
394 were also found but much less numerous; the *FOXL2* labelling was very faint. The diagrams show the results of a
395 quantitative analysis of gene expression. Values are relative expressions measured using total RNA extracted
396 from the two gonads of each animal from wild type (WT), *ARO*$^{+/-}$ (+/-) *and ARO*$^{-/-}$ (-/-) rabbits; the same RNA
397 samples were analyzed in the four diagrams. Horizontal bars represent the medians. The STRA8/DDX4 and
398 SPO11/DDX4 diagrams represent the ratio between the expression of the genes for each sample. Stars represent
399 the statistical significance ($p<0.01$).
400
401 These differences intensified further (supplementary Figure 9). As meiosis progressed (10 days
402 *post partum*, d*pp*), zygotene, pachytene and diplotene stages were simultaneously observed
403 in wild type ovaries. At the interface between the cortex and the medulla, the large ovigerous
404 cords broke down, forming numerous early primordial follicles encompassing diplotene stage
405 germ cells surrounded by a ring of flat pre-granulosa cells. This was far to be observed in *ARO*$^{-}$
406 $^{/-}$ ovaries. Indeed, at 7 days after birth, almost no germ cells in zygotene or pachytene stages
407 were detected; a small number of diplotene-like stage cells were nonetheless detected, some
408 surrounded by a discontinuous ring of somatic cells that could be assumed to be pre-granulosa
409 cells.
410 Later on at 16-19 d*pp*, the gonad size was approximately twice as small in *ARO*$^{-/-}$ rabbits,
411 harboring a thin cortex with a small number of primordial follicles (Figure 10A). All ovigerous
412 cords broke down both in wild type and *ARO*$^{-/-}$ ovaries and follicles were isolated. However,
413 in *ARO*$^{-/-}$ ovaries, the ring of pre-granulosa cells surrounding the oocytes was frequently
414 discontinuous and rare well-developed primordial follicles were detected. The *FOXL2* ISH
415 labelling was very weak reflecting a low level of well-differentiated granulosa cells (Figure
416 10B). Nevertheless, oocytes of primordial follicles were positive for the *RSPO2* ISH specific
417 probe in *ARO*$^{-/-}$ follicles, as in wild type ones (Figure 10C).
418

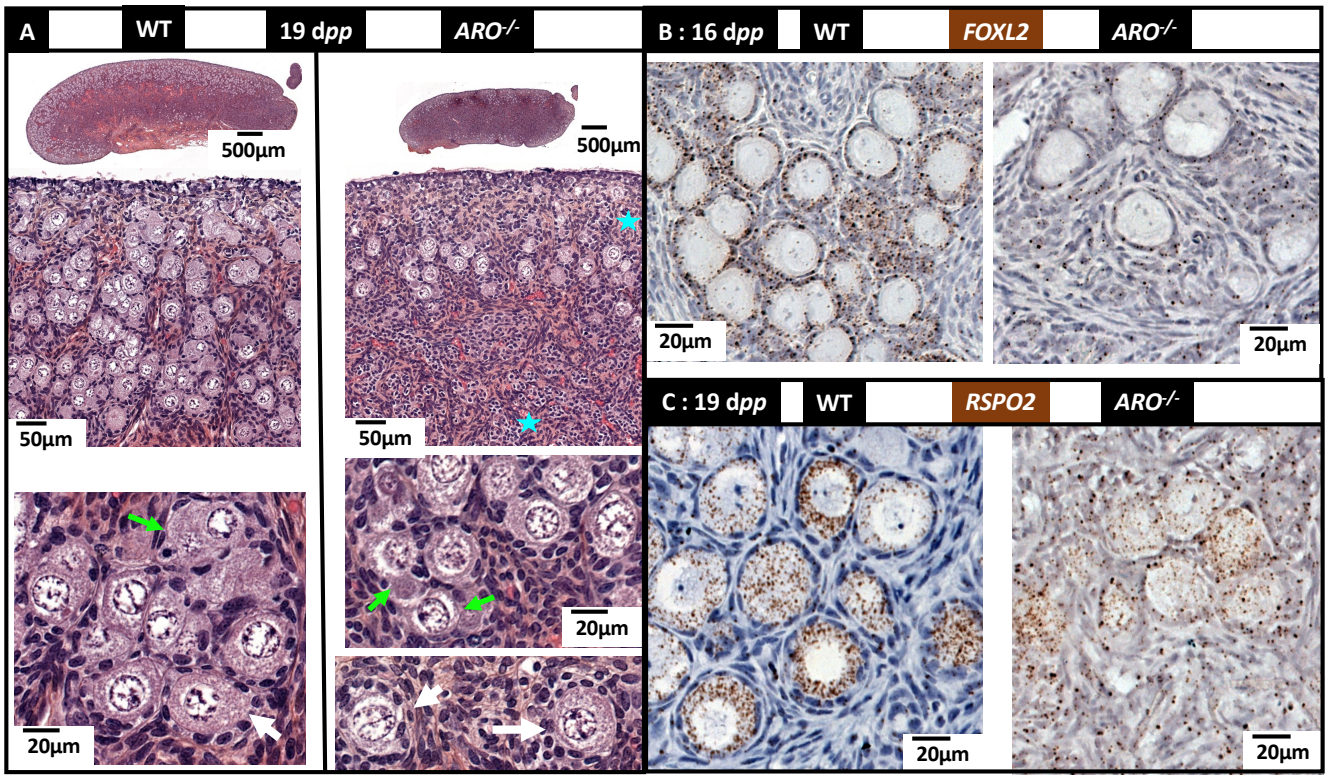

Figure 10: early follicle differentiation. Ovaries were collected at 16 or 19 d*pp* then treated with Bouin's or PAF fixative and processed for HES staining or ISH labelling respectively.

Figure 10: early follicle differentiation. Ovaries were collected at 16 or 19 d*pp* then treated with Bouin's or PAF fixative and processed for HES staining or ISH labelling respectively. **(A): HES staining of 19 d*pp* sections**. Blue stars point the abnormal persistence of connective tissue, void of differentiating oocytes or follicles, at the outer part of the cortex and in the medulla of *ARO*$^{-/-}$ ovaries. The green arrows point some of the primordial follicles in formation with a discontinuous wall of granulosa cells. Early formed primordial follicles surrounded by a wall of regular shape granulosa cells are found in wild type and *ARO*$^{-/-}$ ovaries (white arrows). **(B) and (C): ISH labelling using *FOXL2* and *RSPO2* gene specific probes.** The *FOXL2* and *RSPO2* probes labelled granulosa cells and oocytes respectively in both wild type and *ARO*$^{-/-}$ ovaries. Note the huge decrease of *FOXL2* positive cells in *ARO*$^{-/-}$ ovaries compared to the WT control ones.

To conclude, in the *ARO*$^{-/-}$ ovaries, a small number of oocytes had differentiated after birth; these oocytes were surrounded by a ring of granulosa cells. Despite the probably abnormal differentiation of the latter (shown by the weak expression of the *FOXL2* gene), a small population of primordial follicles could differentiate. At the same time, the ovary was invaded by the connective tissue filled with fibers rich in collagen as previously observed from 20 d*pc* onwards; this latter was not replaced by the ovigerous nests as normally occurs in non-mutant ovaries. The *ARO*$^{-/-}$ ovaries may have failed to fill-in this connective tissue due to the disturbed formation of ovigerous nests.

438

439 **Discussion**

440 The already long-standing demonstration of a peak of *CYP19A1* gene expression, AROMATASE
441 activity and estradiol production by the fetal ovary in several mammal species between the
442 stage of sex determination and the initiation of meiosis has raised questions on the role of
443 locally produced estrogens on the fetal differentiation of this organ. The mouse model was
444 for a long time the sole available model to study the function of genes *in vivo*. So, strains of
445 *Cyp19a1* gene or *estrogen-receptor* genes KO mice have been created and a series of papers
446 have reported their phenotype (Fisher *et al.* 1998; Couse *et al.* 1999; Britt *et al.* 2000; Britt *et*
447 *al.* 2001; Findlay *et al.* 2001; Hamilton *et al.* 2014). All XX mice developed ovaries, but follicle
448 differentiation was abnormal after birth. However, this model could not answer to our
449 question since the mouse is one species where *Cyp19a1* gene expression is detected after
450 meiosis initiation in the "late" fetal ovary (Dutta *et al.* 2014) and not before (Greco and Payne
451 1994). Thanks to the recent possibility to target genome modifications in numerous other
452 species, we created a rabbit model harboring a mutation in the *CYP19A1* gene (*ARO*$^{-/-}$), a
453 species with a peak of *CYP19A1* gene expression in fetal ovary before meiosis. The *ARO*$^{-/-}$
454 rabbits were totally void of any estrogen production. Particularly, the amount of estradiol in
455 gonads of all *ARO*$^{-/-}$ fetuses was undetectable, which eliminates the possibility of any
456 compensatory mechanism through estradiol from maternal or placental origins. More, no
457 testosterone was detected in the *ARO*$^{-/-}$ fetal gonads, thus eliminating any possibility of
458 interference due to the local accumulation of androgens in response to the lack of androgen
459 aromatization. The key results of this study regarding XX *ARO*$^{-/-}$ ovary phenotype were: 1) no
460 XX sex reversal in *ARO*$^{-/-}$ rabbits, 2) an abnormal differentiation of *FOXL2* positive cells, leading
461 to the poor differentiation of ovigerous nests and the reduction of the number of meiotic
462 germ cells and 3) a quasi-absence of follicular reserve, also linked to early folliculogenesis
463 failure.

464

465 **AROMATASE is not an ovarian determining enzyme in mammals**

466 The question of the role of estrogens in sex determination in mammals was prompted by the
467 finding that in goats, the *FOXL2* gene was a main actor for ovarian determination, since the
468 *FOXL2* gene loss of function caused an ovary-to-testis sex reversal of the fetal gonad
469 (Boulanger *et al.* 2014). Previously, FOXL2 was shown to be a crucial transcriptional activator

470 of the *CYP19A1* gene in goats (Pannetier *et al.* 2006) and fishes (Govoroun *et al.* 2004;
471 Pannetier *et al.* 2006; Guiguen *et al.* 2010), and possibly in chicken (Govoroun *et al.* 2004).
472 Thus, the question was raised to know whether FOXL2 could act on sex determination through
473 *CYP19A1* gene transcriptional activation. This question was all the more important that in non-
474 mammalian vertebrate species, anti-aromatase drugs induced female to male sex-reversal
475 (see (Vaillant *et al.* 2001) in the chicken and (Yin *et al.* 2017) in fish). The rabbit was possibly
476 an interesting model since, as in goats, the surge of expression of the *FOXL2* gene in the fetal
477 ovary occurs when starts the peak of *CYP19A1* gene expression at the gonadal sex
478 determination (Diaz-Hernandez *et al.* 2008; Daniel-Carlier *et al.* 2013). The results of the
479 present study demonstrate that estrogens play no role on the female/male determinism of
480 the rabbit gonad. A similar finding had already been described in humans, where several cases
481 of total *CYP19A1* gene inactivation were reported (Akcurin *et al.* 2016; Zhu *et al.* 2016; Mazen
482 *et al.* 2017; Unal *et al.* 2018; Praveen *et al.* 2020). In spite of numerous symptoms affecting
483 the development of gonads, of external genitalia and of breast in the girl, with multiple
484 disorders in energy and bone metabolisms, there was no sex reversal of the human ovary as
485 regard to the genetic sex (Zhu *et al.* 2016). In contrast, opposite data were reported in the
486 mouse species, describing an increase in the serum testosterone levels in *Cyp19a1*$^{-/-}$ females
487 (Fisher *et al.* 1998) and the presence of seminiferous-like structures in the gonads of adult
488 *Esr1/Esr2* double knock out females (Couse *et al.* 1999; Amano *et al.* 2017). However, this has
489 been controversial and not found by all authors.
490
491 **Estrogens are involved in early ovarian development**
492 The fetal ovarian differentiation is known to be intimately linked to mechanisms that involve
493 cellular interactions and cell migration, depending on autocrine and paracrine signaling
494 pathways. These processes involve genes coding for the components of the extracellular
495 matrix and cell-cell adhesion molecules. Estrogens have been reported as potent actors in
496 these mechanisms (Juengel *et al.* 2002; Gentilini *et al.* 2007; Wilhelm *et al.* 2007; Zalewski *et*
497 *al.* 2012; Hummitzsch *et al.* 2013). The reduced size of the gonads together with the reduced
498 number of somatic and germ cells is one of the major characteristics of the *ARO*$^{-/-}$ rabbit
499 ovaries. It was detected shortly after gonadal sex determination (18 d*pc*), and still clearly
500 visible around birth with a dramatic decrease of ovarian nests. We have also shown that the
501 estrogen receptor α gene (*ESR1*) was strongly expressed by the ovarian cortical cells

502 specifically by cells located within the coelomic epithelium (Figure 5B). This is worth to be
503 pointed out because it resembles to what has been described in chicken. Indeed, in this
504 species the female to male sex reversal induced by the AROMATASE inhibitor fadrozole
505 induced a reduction of *FOXL2* expression (Hudson *et al.* 2005). More, the experimental down-
506 regulation of the epithelial *Esr*α gene was sufficient to severely affect the ovarian cortex
507 differentiation (Guioli *et al.* 2020), thus suggesting that the natural absence of *Esr*α expression
508 in the cortex of the right ovary of the hen was at least partially responsible for the asymmetric
509 degeneration of the right ovary (Guioli *et al.* 2014). We can therefore hypothesize that in
510 rabbit *ARO*$^{-/-}$ ovaries, the absence of estrogens can lead to a dramatic decrease of proliferative
511 activity in the coelomic epithelium, evidenced by the KI67 staining (Figure 7A) and by the
512 decrease of *FOXL2*-expressing somatic cells from 20-22 d*pc* (Figure 6).
513 Anyway, without estrogens, the proliferation of ovarian cells seemed to be affected but not
514 abolished since some nests were clearly visible in *ARO*$^{-/-}$ gonads at birth although under-
515 developed. So, given that estrogens are involved in ovigerous nests formation, other factors
516 are likely to play a role in this process as well. It has been shown in mice that the
517 *Rspo1/Wnt4/*β*-catenin* pathway is involved in cell proliferation of the coelomic epithelium of
518 both sexes during the gonadal switch (Chassot *et al.* 2012). This pathway could thus be
519 responsible at least in part of the formation of the few ovigerous nests in *ARO*$^{-/-}$ rabbit ovaries.
520 Transcriptomics (even at the single cell level) and epigenetics studies are underway on WT
521 rabbit ovaries in our team to search molecular targets of estrogens in early ovarian
522 development by comparison with *ARO*$^{-/-}$ gonads.
523
524 **The number of germ cells was affected by the lack of estrogens.**
525 The reduced number of germ cells is one of the major characteristics of the *ARO*$^{-/-}$ rabbit
526 ovaries. One of the first sign was the low expression level of the pluripotency marker gene
527 *OCT4* and its reduced ISH labelling (see Figures 5 and 6). In mammals, germ cells colonize early
528 the genital crests (Juengel *et al.* 2002; Wilhelm *et al.* 2007; Hummitzsch *et al.* 2013). In the
529 rabbit species, it starts at 9 d*pc* and is over at around 18 d*pc* (Chretien 1966). Since the
530 *CYP19A1* gene expression starts at 18 d*pc*, it is likely that the germ cell colonization occurs
531 independently of *CYP19A1* expression. Thus, in the *ARO*$^{-/-}$ ovary, in spite of the absence of
532 estradiol, the initial stock of germ cells was probably not altered. In mammalian ovaries, once
533 germ cells enter the genital ridges, they multiply intensely by mitosis until meiosis. Then, the

534 number of germ cells does not increase any more. Numerous articles have shown that in
535 mammals estrogens stimulate the mitotic activity in the fetal ovary (see review in (Auersperg
536 *et al.* 2001; Chou and Chen 2018)). During fetal life in rabbits, the mitotic activity of germ cells,
537 which is maximum around 16-18 d*pc*, remains high up to 26 d*pc* (Chretien 1966), when the
538 *CYP19A1* and *ESR1* genes are strongly expressed (Supplementary Figure 7). It can be suggested
539 that the estradiol produced by AROMATASE in the fetal ovary could regulate the mitotic
540 activity of germ cells. This hypothesis is supported by the fact that the germ cells, labelled at
541 this stage by the *OCT4* HIS probe, were co-localized in the surface epithelium with cells
542 expressing the *ESR1* gene. Germ cell death has previously been reported to occur continuously
543 in the ovary from early fetal stages until puberty and later on (Hussein 2005; Myers *et al.*
544 2014). In *ARO*$^{-/-}$ ovaries, the number of γH2AX positive germ cells (highlighting DNA
545 fragmentation, and at this stage dying germ cells) was similar to that in wild type ones (Figure
546 7). Thus, our data suggest that this is probably not germ cell death but rather the lack of germ
547 cell divisions that was responsible for the low number of germ cells in the early *ARO*$^{-/-}$ ovary
548 before meiosis.
549
550 **Germ cells were committed in meiosis in spite of the lack of estrogens.**
551 The commitment of germ cells in meiosis marks the first step of their differentiation as
552 oocytes. In the rabbit species, it occurs at the third part of pregnancy (at around 28 d*pc*), and
553 is characterized by the surge of the *STRA8* gene expression in germ cells specifically.
554 Interestingly, in the *ARO*$^{-/-}$ ovaries, numerous germ cells were committed to meiosis as shown
555 by the significant surge of *STRA8* gene expression; more, the various steps of the meiotic
556 prophase were distinguishable, and the meiosis specific maker gene *SPO11* was significantly
557 expressed as well. Thus, it suggests that nor the estradiol neither the AROMATASE enzyme
558 were necessary for meiotic induction and progression. As discussed previously, the number of
559 germ cells possible to be committed in meiosis was reduced in *ARO*$^{-/-}$ ovaries. More, it should
560 be pointed out that the ratio of gene expression *STRA8/DDX4* and *SPO11/DDX4* was low in
561 *ARO*$^{-/-}$ ovaries, showing that an abnormal loss of germ cells occurred at commitment or during
562 meiosis. Thus, although estrogens are not mandatory for meiosis commitment, the fact
563 remains that they are important for limiting meiotic germ cell losses.
564
565 **Estrogens deprivation impacts follicle formation**

566 Another key feature of the phenotype of the *ARO*$^{-/-}$ females concerns the abnormal genital
567 tract and ovarian follicle differentiation. At puberty, the genital tract of the XX *ARO*$^{-/-}$ rabbit
568 was profoundly altered, with massive atrophy, as already reported in *Cyp19a1*$^{-/-}$ mice (Fisher
569 *et al.* 1998; Britt *et al.* 2000), and in agreement with the fact already demonstrated that the
570 development of the female genital tract is highly dependent on estrogens. The follicle
571 differentiation that starts 12-15 days after birth in rabbit at the arrest of meiosis prophase is
572 a continuous process that involves the surrounding of oocytes with flat pre-granulosa cells
573 and the breakdown of ovigerous nests thus giving rise to primordial follicles. Then, the
574 differentiation of pre-granulosa cells from flat- to cuboidal-form cells signs the differentiation
575 of primary follicles. Of course, the size of the population of primordial follicles is linked to the
576 number of oocytes, the latter being the consequence of all the events which occurred during
577 fetal and neonatal life as discussed previously. In the *ARO*$^{-/-}$ rabbit ovary, this is of particular
578 importance since the pool of oocytes and that of *FOXL2* expressing pre-granulosa cells are
579 extremely reduced. More, it has been reported that the nests breakdown is an event
580 specifically sensitive to apoptotic losses (Myers *et al.* 2014). This could explain why the pool
581 of primordial follicles was very low in *ARO*$^{-/-}$ rabbit ovary few days after birth (Figure 10) and
582 almost null at puberty (Figure 2). The poor expression of the *FOXL2* marker gene by the
583 granulosa cells 16 days after birth signs the abnormal differentiation of the primary follicles,
584 the number of which was extremely low (Figure 2). Surprisingly, controversial results were
585 reported in *Cyp19a1* KO mice, where the number of primary follicles was significantly higher
586 than in wild type mice (Britt *et al.* 2000). To date, we have no explanation for such differences.
587 Furthermore, we observed that despite the absence of estradiol, large antral follicles with
588 oocytes developed in the *ARO*$^{-/-}$ ovary, however these follicles were very few. This proves that
589 estrogens are not the only actors in follicular growth and differentiation at puberty and
590 onwards. Many previous studies have shown that these events depend on the interactions
591 between several signaling pathways, among which are estrogens but also the anti-Müllerian
592 hormone (AMH) and gonadotropins (Grynberg *et al.* 2012; Dewailly *et al.* 2016; Chou and Chen
593 2018). Additional studies are underway to further analyze the mechanisms of differentiation
594 of these follicles in the absence of estradiol.
595
596 To conclude, the present work shows that in the rabbit species, the *CYP19A1* gene mutation
597 and the absence of estrogens from early embryo life was at the source of a series of main

598 disorders of the ovarian differentiation process. It did not disturb the sex determination of the
599 early fetal gonad but impacted profoundly the number of germ cells and the early
600 differentiation of somatic cells. It then had repercussions on the subsequent follicular growth
601 and differentiation and finally led to female infertility. This paper brings major and original
602 data on the role of estrogens in species where the *CYP19A1* gene is expressed in the fetal
603 ovary before meiosis. Deciphering the gene pathways sensitive to estrogens is currently
604 underway in our team in order to better understand specifically the role of endocrine
605 disruptors such as xeno-estrogens on female fertility.
606

607 **Materials and methods**

608 **Animals**

609 New Zealand rabbits (NZ1777, Hypharm, Rousssay, France) were bred at the SAAJ rabbit
610 facility (Jouy-en-Josas, France). All experiments were performed with the approval of the
611 French Ministry MENESR (accreditation number APAFIS#6775-2016091911407980 vI) following
612 the recommendation given by the local committee for ethic in animal experimentation
613 (COMETHEA, Jouy-en-Josas). All researchers working directly with the animals possessed an
614 animal experimentation license delivered by the French veterinary services. Hormonal
615 treatments for superovulation and surgery for embryo transfer were performed as previously
616 described (Peyny *et al.* 2020).

617

618 **Design of TALEN sequences and plasmid constructions**

619 Exon II of rabbit AROMATASE gene was targeted to create InDel mutations near the site of
620 initiation of translation (ATG site). The target sequences (left arm: 5'-TGCTTCATCTGAAGCCA-
621 3' (sense); right arm: 5'-TGGGTTCAGTATTTCCA-3' (antisense); 16 bases spaced) were chosen
622 with the ZiFiT Targeter sofware (http://zifit.partners.org). No homology was identified at any
623 other location in the rabbit genome that could represent a potential off-target site
624 (supplementary table 1). The TALEN were constructed as described (Sander *et al.* 2011), see
625 in supplementary methods). Each TALEN RNA was diluted (100 ng/µl) in injection buffer
626 (Millipore, France) and stored at -80°C until used.

627

628 **Generation of mutant rabbits**

629 Embryos produced from superovulated females were injected at single-cell stage with an
630 equimolar mixture of the left and right arm TALEN mRNAs (50ng/µl each). Injected embryos
631 were implanted 3-4 hours after injection into the oviducts of anesthetized recipient rabbits
632 via laparotomy. For all details concerning handling of females and embryos, see in (Peyny *et*
633 *al.* 2020).

634 Offspring were screened for the presence of InDel mutations using genomic DNA extracted
635 from ear clips (Jolivet *et al.* 2014). First detection of founders and characterization of mutation
636 were performed using one set of primers located far upstream and downstream the targeted
637 ATG (F0/R0, Figure 1 and supplementary table 2 for all primer sequences). The amplified
638 fragments were sequenced (Eurofins Genomics, Courtaboeuf, France) and the extent of the
639 mutation was deduced by comparing with the sequence of a wild type rabbit.

640 For further routine screening of mutants, a quantitative PCR (Fast SYBR Green Master Mix,
641 Applied Biosystems, ThermoFisher, France) was performed using two sets of primers, the
642 *CYP19A1* specific one (*CYP19A1* gene specific primers) flanking the position of the
643 characterized InDel mutations (F1/R1, supplementary table 2) and another set to amplify a 2
644 copies reference gene (the rabbit *beta GLOBIN* gene, ENSOCUG00000000568). By using the
645 $\Delta(\Delta Ct)$ method with a wild type rabbit DNA as reference DNA, we deduced the copy number
646 of the *CYP19A1* allele in each DNA sample (no amplification = the two alleles are mutant (ARO^{-}
647 $^{/-}$ genotype); one copy = one mutant allele ($ARO^{-/+}$ genotype); two copies = wild type (WT or
648 $ARO^{+/+}$ genotype).

649 The presence/absence of the Y chromosome was deduced from the amplification of the *SRY*
650 gene through PCR analyses with the rabbit *beta GLOBIN* gene as positive control of the PCR
651 and *SRY* specific primers (supplementary table 2). All rabbits were tested to determine the
652 genomic sex in parallel to the external and histological observations. In the present paper,
653 mentions of the XY or XX genotype always refer to the PCR determination.

654

655 **Histological and immunohistological analyses**

656 Immediately after sampling, gonads were immersed in Bouin's fixative or paraformaldehyde
657 (4% PAF in PBS 1x), fixed for 24 to 72 hours then paraffin embedded. Microtome sections of
658 5µm thickness were processed. Hematoxylin-eosin-saffron (HES) colorations were performed

659 by the @Bridge platform (INRAE, Jouy-en-Josas) using an automatic Varistain Slide Stainer
660 (Thermo Fisher Scientific). Sirius Red-Fast Green colorations were performed manually.
661 In situ hybridization (ISH) was performed using the RNAscope ISH methodology (ACD, Bio-
662 Techne SAS, Rennes, France). Briefly, probes at around 1000nt long were designed and
663 produced by the manufacturer in order to match to the full-length cDNA of interest, taking
664 care to reduce any cross-hybridization with non-specific targets. The list of all synthesized
665 probes is given in supplementary table 3. Hybridization was performed on 5µm sections from
666 PAF fixed tissue using labelling kits (RNAscope 2.5HD assay-brown or -red, or RNAscope 2.5HD
667 duplex chromogenic assay blue (conjugated to horse radish peroxidase) and red (conjugated
668 to alkaline phosphatase)) as recommended by the manufacturer. The red labelling (Fast Red)
669 was observed as visible or fluorescent signals. Hybridization was considered as positive when
670 at least one dot was observed in one cell.
671 Immunohistological analyses were performed on 5µm sections from PAF fixed tissue. The
672 supplementary table 4 recapitulates the antibodies used.
673 All colored sections (visible, or fluorescent ones) were scanned using a 3DHISTECH panoramic
674 scanner at the @Bridge platform (INRAE, Jouy-en-Josas).
675
676 **RNA extraction and RT-qPCR analyses**
677 Gonads from rabbit fetuses were collected and immediately frozen at -80°C. Total RNA from
678 each gonad was extracted using the RNeasy® MicroKit (Qiagen, France). Quantitative PCR was
679 performed on reverse transcribed RNAs (High Capacity Reverse cDNA Transcription kit with
680 the included set of random primers, Applied Biosystems, ThermoFisher, France). Several PCR
681 sets of primers and analyses were those published previously (Daniel-Carlier *et al.* 2013).
682 Other sets of primers are given in the supplementary table 2. Data from significant and specific
683 amplifications only were reported, thus excluding all amplifications with too high or variable
684 C_t values, and non-specific or multiple amplifications.
685
686 **Measurement of estradiol, testosterone and anti Mülllerian hormone levels in serum**
687 **samples and fetal gonads**
688 Estradiol and testosterone were assayed by GC/MS according to the protocol described by
689 Giton et al. (Giton *et al.* 2015) with modifications (Devillers *et al.* 2019). Female rabbit serum
690 from *ARO*$^{-/-}$ genotype was used as the matrix for calibrators and quality control (QC) standards

691 after twice charcoal dextran treatments. Sample extraction and purification, derivatization
692 and determination of estradiol and testosterone levels in serum samples and fetal gonads are
693 described in details as supplementary information (see also supplementary Table 5) or can be
694 provided upon request. Anti Müllerian hormone levels were determined in 50 µl aliquots of
695 serum samples by using an ELISA kit (AMH GenII ELISA, with AMH Gen II calibrators and
696 controls, Beckman Coulter, Villepinte, France) as previously described (Bourdon *et al.* 2018).
697
698 **Statistics**
699 The statistical analyses were performed using the GraphPad Prism 7 Software (GraphPad
700 Software Inc., La Jolla, CA, USA). Because of the small number of samples in groups,
701 comparisons between values were made by the Mann-Whitney test for non-parametric
702 values. A probability lower than 0.05 was required for significance.
703
704 **Acknowledgements**
705 The authors would like to thank the staff of the facility (SAAJ, INRAE, Jouy-en-Josas) for the
706 care of the rabbits and Julie Rivière and Marthe Vilotte (UMR GABI, INRAE, Jouy-en-Josas) for
707 their assistance on the histological plateau (@Bridge platform) and for the access to the virtual
708 slide scanner (MIMA2 platform). Special thanks go to Danielle Monniaux (UMR PRC, INRAE,
709 Nouzilly) for the time she spent in enriching discussions and highly valuable comments. This
710 study was supported by ANR grants (GENIDOV:ANR-09-GENM-009; ARGONADS: ANR-13-
711 BSV2-0017; ARDIGERM: ANR-2020-CE14). The authors declare that they have no competing
712 interests.
713

714 References
715
716 Akcurin, S., Turkkahraman, D., Kim, W.Y., Durmaz, E., Shin, J.G., and Lee, S.J. (2016) A
717 Novel Null Mutation in P450 Aromatase Gene (CYP19A1) Associated with Development of
718 Hypoplastic Ovaries in Humans. *J Clin Res Pediatr Endocrinol* **8**(2), 205-10
719
720 Amano, A., Kondo, Y., Noda, Y., Ohta, M., Kawanishi, N., Machida, S., Mitsuhashi, K.,
721 Senmaru, T., Fukui, M., Takaoka, O., Mori, T., Kitawaki, J., Ono, M., Saibara, T., Obayashi,
722 H., and Ishigami, A. (2017) Abnormal lipid/lipoprotein metabolism and high plasma
723 testosterone levels in male but not female aromatase-knockout mice. *Arch Biochem Biophys*
724 **622**, 47-58
725
726 Auersperg, N., Wong, A.S.T., Choi, K.-C., Kang, S.K., and Leung, P.C.K. (2001) Ovarian
727 Surface Epithelium: Biology, Endocrinology, and Pathology*. *Endocr Rev* **22**(2), 255-288
728
729 Boulanger, L., Pannetier, M., Gall, L., Allais-Bonnet, A., Elzaiat, M., Le Bourhis, D., Daniel,
730 N., Richard, C., Cotinot, C., Ghyselinck, N.B., and Pailhoux, E. (2014) FOXL2 is a female sex-
731 determining gene in the goat. *Curr Biol* **24**(4), 404-8
732
733 Bouraïma, H., Hanoux, V., Mittre, H., Féral, C., Benhaïm, C., and Leymarie, P. (2001)
734 Expression of tthe rabbit cytochroma P450 aromatase encoding gene uses alternative tissue-
735 specific promoters. *Eur. J. Biochem.* **268**, 4506-4512
736
737 Bourdon, M., Torres-Rovira, L., Monniaux, D., Faure, C., Levy, R., Tarrade, A., Rousseau-
738 Ralliard, D., Chavatte-Palmer, P., and Jolivet, G. (2018) Impact of a gestational exposure to
739 diesel exhaust on offspring gonadal development: experimental study in the rabbit. *J Dev Orig*
740 *Health Dis* **9**(5), 519-529
741
742 Britt, K.L., Drummond, A.E., Cox, V.A., Dyson, M., Wreford, N.G., Jones, M.E., Simpson,
743 E.R., and Findlay, J.K. (2000) An age-related ovarian phenotype in mice with targeted
744 disruption of the Cyp 19 (aromatase) gene. *Endocrinology* **141**(7), 2614-23
745
746 Britt, K.L., Drummond, A.E., Dyson, M., Wreford, N.G., Jones, M.E., Simpson, E.R., and
747 Findlay, J.K. (2001) The ovarian phenotype of the aromatase knockout (ArKO) mouse. *J*
748 *Steroid Biochem Mol Biol* **79**(1-5), 181-5
749
750 Chassot, A.A., Bradford, S.T., Auguste, A., Gregoire, E.P., Pailhoux, E., de Rooij, D.G.,
751 Schedl, A., and Chaboissier, M.C. (2012) WNT4 and RSPO1 together are required for cell
752 proliferation in the early mouse gonad. *Development* **139**(23), 4461-72
753
754 Chou, C.H., and Chen, M.J. (2018) The Effect of Steroid Hormones on Ovarian Follicle
755 Development. *Vitam Horm* **107**, 155-175
756
757 Chretien, F.C. (1966) [A study of the origin, migration and multiplication of the germ-cells of
758 the rabbit embryo]. *J Embryol Exp Morphol* **16**(3), 591-607
759
760 Conley, A., and Hinshelwood, M. (2001) Mammalian aromatases. *Reproduction* **121**(5), 685-
761 95
762

763 Couse, J.F., Hewitt, S.C., Bunch, D.O., Sar, M., Walker, V.R., Davis, B.J., and Korach, K.S.
764 (1999) Postnatal sex reversal of the ovaries in mice lacking estrogen receptors alpha and beta.
765 *Science* **286**(5448), 2328-31
766
767 Daniel-Carlier, N., Harscoet, E., Thepot, D., Auguste, A., Pailhoux, E., and Jolivet, G. (2013)
768 Gonad differentiation in the rabbit: evidence of species-specific features. *PLoS One* **8**(4),
769 e60451
770
771 Devillers, M.M., Petit, F., Cluzet, V., Francois, C.M., Giton, F., Garrel, G., Cohen-Tannoudji,
772 J., and Guigon, C.J. (2019) FSH inhibits AMH to support ovarian estradiol synthesis in infantile
773 mice. *J Endocrinol* **240**(2), 215-228
774
775 Dewailly, D., Robin, G., Peigne, M., Decanter, C., Pigny, P., and Catteau-Jonard, S. (2016)
776 Interactions between androgens, FSH, anti-Müllerian hormone and estradiol during
777 folliculogenesis in the human normal and polycystic ovary. *Hum Reprod Update* **22**(6), 709-
778 724
779
780 Diaz-Hernandez, V., Leon del Rio, A., Zamora, M., and Merchant-Larios, H. (2008) Expression
781 profiles of SRY and SOX9 in rabbit gonads: the classical model of mammalian sex
782 differentiation. *Sex Dev* **2**(3), 152-66
783
784 Dickmann, Z., Dey, S.K., and Gupta, J.S. (1975) Steroidogenesis in rabbit preimplantation
785 embryos. *Proc Natl Acad Sci U S A* **72**(1), 298-300
786
787 Dutta, S., Mark-Kappeler, C.J., Hoyer, P.B., and Pepling, M.E. (2014) The steroid hormone
788 environment during primordial follicle formation in perinatal mouse ovaries. *Biol Reprod*
789 **91**(3), 68
790
791 Elbrecht, A., and Smith, R.G. (1992) Aromatase enzyme activity and sex determination in
792 chickens. *Science* **255**(5043), 467-70
793
794 Findlay, J.K., Britt, K., Kerr, J.B., O'Donnell, L., Jones, M.E., Drummond, A.E., and Simpson,
795 E.R. (2001) The road to ovulation: the role of oestrogens. *Reprod Fertil Dev* **13**(7-8), 543-7
796
797 Fisher, C.R., Graves, K.H., Parlow, A.F., and Simpson, E.R. (1998) Characterization of mice
798 deficient in aromatase (ArKO) because of targeted disruption of the cyp19 gene. *Proc Natl*
799 *Acad Sci U S A* **95**(12), 6965-70
800
801 Gadsby, J.E., Heap, R.B., and Burton, R.D. (1980) Oestrogen production by blastocyst and
802 early embryonic tissue of various species. *J Reprod Fertil* **60**(2), 409-17
803
804 Garverick, H.A., Juengel, J.L., Smith, P., Heath, D.A., Burkhart, M.N., Perry, G.A., Smith,
805 M.F., and McNatty, K.P. (2010) Development of the ovary and ontongeny of mRNA and
806 protein for P450 aromatase (arom) and estrogen receptors (ER) alpha and beta during early fetal
807 life in cattle. *Anim Reprod Sci* **117**(1-2), 24-33
808
809 Gentilini, D., Busacca, M., Di Francesco, S., Vignali, M., Vigano, P., and Di Blasio, A.M.
810 (2007) PI3K/Akt and ERK1/2 signalling pathways are involved in endometrial cell migration
811 induced by 17beta-estradiol and growth factors. *Mol Hum Reprod* **13**(5), 317-22
812

George, F.W., Milewitch, L., and Wilson, J.D. (1978) Oestrogen content of the embryonic rabbit ovary. *Nature* **274**, 172-173

George, F.W., and Wilson, J.D. (1978a) Conversion of Androgen to Estrogen by the Human Fetal Ovary. *J Clin Endocr Metab* **47**, 550-555

George, F.W., and Wilson, J.D. (1978b) Estrogen formation in the early rabbit embryo. *Science* **199**, 200-201

Giton, F., Sirab, N., Franck, G., Gervais, M., Schmidlin, F., Ali, T., Allory, Y., de la Taille, A., Vacherot, F., Loric, S., and Fiet, J. (2015) Evidence of estrone-sulfate uptake modification in young and middle-aged rat prostate. *J Steroid Biochem Mol Biol* **152**, 89-100

Gondos, B., George, F., and Wilson, J. (1983) Granulosa cell differentiation and estrogen synthesis in the fetal rabbit ovary. *Biol Reprod* **29**(3), 791-798

Govoroun, M.S., Pannetier, M., Pailhoux, E., Cocquet, J., Brillard, J.P., Couty, I., Batellier, F., and Cotinot, C. (2004) Isolation of chicken homolog of the FOXL2 gene and comparison of its expression patterns with those of aromatase during ovarian development. *Dev Dyn* **231**(4), 859-70

Greco, T.L., and Payne, A.H. (1994) Ontogeny of expression of the genes for steroidogenic enzymes P450 side-chain cleavage, 3 beta-hydroxysteroid dehydrogenase, P450 17 alpha-hydroxylase/C17-20 lyase, and P450 aromatase in fetal mouse gonads. *Endocrinology* **135**(1), 262-8

Grynberg, M., Pierre, A., Rey, R., Leclerc, A., Arouche, N., Hesters, L., Catteau-Jonard, S., Frydman, R., Picard, J.Y., Fanchin, R., Veitia, R., di Clemente, N., and Taieb, J. (2012) Differential regulation of ovarian anti-mullerian hormone (AMH) by estradiol through alpha- and beta-estrogen receptors. *J Clin Endocr Metab* **97**(9), E1649-57

Guiguen, Y., Fostier, A., Piferrer, F., and Chang, C.F. (2010) Ovarian aromatase and estrogens: a pivotal role for gonadal sex differentiation and sex change in fish. *Gen Comp Endocrinol* **165**(3), 352-66

Guioli, S., Nandi, S., Zhao, D., Burgess-Shannon, J., Lovell-Badge, R., and Clinton, M. (2014) Gonadal asymmetry and sex determination in birds. *Sex Dev* **8**(5), 227-42

Guioli, S., Zhao, D., Nandi, S., Clinton, M., and Lovell-Badge, R. (2020) Oestrogen in the chick embryo can induce chromosomally male ZZ left gonad epithelial cells to form an ovarian cortex that can support oogenesis. *Development* **147**(4)

Hamilton, K.J., Arao, Y., and Korach, K.S. (2014) Estrogen hormone physiology: reproductive findings from estrogen receptor mutant mice. *Reprod Biol* **14**(1), 3-8

Hudson, Q.J., Smith, C.A., and Sinclair, A.H. (2005) Aromatase inhibition reduces expression of FOXL2 in the embryonic chicken ovary. *Dev Dyn* **233**(3), 1052-5

861 Hummitzsch, K., Irving-Rodgers, H.F., Hatzirodos, N., Bonner, W., Sabatier, L., Reinhardt,
862 D.P., Sado, Y., Ninomiya, Y., Wilhelm, D., and Rodgers, R.J. (2013) A new model of
863 development of the mammalian ovary and follicles. *PLoS One* **8**(2), e55578
864
865 Hussein, M.R. (2005) Apoptosis in the ovary: molecular mechanisms. *Hum Reprod Update*
866 **11**(2), 162-77
867
868 Jolivet, G., Braud, S., DaSilva, B., Passet, B., Harscoet, E., Viglietta, C., Gautier, T., Lagrost,
869 L., Daniel-Carlier, N., Houdebine, L.M., and Harosh, I. (2014) Induction of body weight loss
870 through RNAi-knockdown of APOBEC1 gene expression in transgenic rabbits. *PLoS One* **9**(9),
871 e106655
872
873 Juengel, J.L., Sawyer, H.R., Smith, P.R., Quirke, L.D., Heath, D.A., Lun, S., Wakefield, S.J.,
874 and McNatty, K.P. (2002) Origins of follicular cells and ontogeny of steroidogenesis in ovine
875 fetal ovaries. *Mol Cell Endocrinol* **191**(1), 1-10
876
877 Kaur, J., and Bose, H.S. (2014) Passenger protein determines translocation versus retention in
878 the endoplasmic reticulum for aromatase expression. *Mol Pharmacol* **85**(2), 290-300
879
880 Lee, J.G., Sung, Y.H., and Baek, I.-J. (2018) Generation of genetically-engineered animals
881 using engineered endonucleases. *Arch Pharm Res* **41**(9), 885-897
882
883 Lee, V.H., Britt, J.H., and Dunbar, B.S. (1996) Localization of laminin proteins during early
884 follicular development in pig and rabbit ovaries. *J Reprod Fertil* **108**(1), 115-22
885
886 Mauleon, P., Bezard, J., and Terqui, M. (1977) Very early and transient 17β-estradiol secretion
887 by fetalsheep ovary. In vitro study. . *Ann Biol Anim Bioch Bioph* **17**, 399-401
888
889 Mazen, I., McElreavey, K., Elaidy, A., Kamel, A.K., and Abdel-Hamid, M.S. (2017) Aromatase
890 Deficiency due to a Homozygous CYP19A1 Mutation in a 46,XX Egyptian Patient with
891 Ambiguous Genitalia. *Sex Dev* **11**(5-6), 275-279
892
893 Myers, M., Morgan, F.H., Liew, S.H., Zerafa, N., Gamage, T.U., Sarraj, M., Cook, M., Kapic,
894 I., Sutherland, A., Scott, C.L., Strasser, A., Findlay, J.K., Kerr, J.B., and Hutt, K.J. (2014)
895 PUMA regulates germ cell loss and primordial follicle endowment in mice. *Reproduction*
896 **148**(2), 211-9
897
898 Pannetier, M., Fabre, S., Batista, F., Kocer, A., Renault, L., Jolivet, G., Mandon-Pepin, B.,
899 Cotinot, C., Veitia, R., and Pailhoux, E. (2006) FOXL2 activates P450 aromatase gene
900 transcription: towards a better characterization of the early steps of mammalian ovarian
901 development. *J Mol Endocrinol* **36**(3), 399-413
902
903 Payen, E., Pailhoux, E., Abou Merhi, R., Gianquinto, L., Kirszenbaum, M., Locatelli, A., and
904 Cotinot, C. (1996) Characterization of ovine SRY transcript and developmental expression of
905 genes involved in sexual differentiation. *Int J Dev Biol* **40**(3), 567-75
906
907 Peters, H., Levy, E., and Crone, M. (1965) Oogenesis in Rabbits. *J Exp Zool* **158**, 169-79
908
909 Peyny, M., Jarrier-Gaillard, P., Boulanger, L., Daniel, N., Lavillatte, S., Cadoret, V., Papillier,
910 P., Monniaux, D., Peynot, N., Duranthon, V., Jolivet, G., and Dalbies-Tran, R. (2020)

Investigating the role of BCAR4 in ovarian physiology and female fertility by genome editing in rabbit. *Sci Rep* **10**(1), 4992

Praveen, V.P., Ladjouze, A., Sauter, K.S., Pulickal, A., Katharopoulos, E., Trippel, M., Perren, A., Pandey, A.V., and Fluck, C.E. (2020) Novel CYP19A1 Mutations Extend the Genotype-Phenotype Correlation and Reveal the Impact on Ovarian Function. *J Endocr Soc* **4**(4), bvaa030

Ross, D.G., Bowles, J., Hope, M., Lehnert, S., and Koopman, P. (2009) Profiles of gonadal gene expression in the developing bovine embryo. *Sex Dev* **3**(5), 273-83

Sander, J.D., Cade, L., Khayter, C., Reyon, D., Peterson, R.T., Joung, J.K., and Yeh, J.R. (2011) Targeted gene disruption in somatic zebrafish cells using engineered TALENs. *Nat Biotechnol* **29**(8), 697-8

Shemesh, M. (1980) Estradiol-17 beta biosynthesis by the early bovine fetal ovary during the active and refractory phases. *Biol Reprod* **23**(3), 577-82

Torley, K.J., da Silveira, J.C., Smith, P., Anthony, R.V., Veeramachaneni, D.N., Winger, Q.A., and Bouma, G.J. (2011) Expression of miRNAs in ovine fetal gonads: potential role in gonadal differentiation. *Reprod Biol Endocrinol* **9**, 2

Unal, E., Yildirim, R., Tas, F.F., Demir, V., Onay, H., and Haspolat, Y.K. (2018) Aromatase Deficiency due to a Novel Mutation in CYP19A1 Gene. *J Clin Res Pediatr Endocrinol*

Vaillant, S., Dorizzi, M., Pieau, C., and Richard-Mercier, N. (2001) Sex reversal and aromatase in chicken. *J Exp Zool* **290**(7), 727-40

Wilhelm, D., Palmer, S., and Koopman, P. (2007) Sex determination and gonadal development in mammals. *Physiol Rev* **87**(1), 1-28

Yin, Y., Tang, H., Liu, Y., Chen, Y., Li, G., Liu, X., and Lin, H. (2017) Targeted Disruption of Aromatase Reveals Dual Functions of cyp19a1a During Sex Differentiation in Zebrafish. *Endocrinology* **158**(9), 3030-3041

Zalewski, A., Cecchini, E.L., and Deroo, B.J. (2012) Expression of extracellular matrix components is disrupted in the immature and adult estrogen receptor beta-null mouse ovary. *PLoS One* **7**(1), e29937

Zhu, W.J., Cheng, T., Zhu, H., Han, B., Fan, M.X., Gu, T., Zhao, S.X., Liu, Y., Cheng, K.X., Song, H.D., and Qiao, J. (2016) Aromatase deficiency: a novel compound heterozygous mutation identified in a Chinese girl with severe phenotype and obvious maternal virilization. *Mol Cell Endocrinol* **433**, 66-74